ELEMENTA
Science of the Anthropocene

RESEARCH ARTICLE

Influence of altered freshwater discharge on the seasonality of nutrient distributions near La Grande River, northeastern James Bay, Québec

Alessia C. Guzzi[1],* , Jens K. Ehn[1], Christine Michel[2], Jean-Éric Tremblay[3], Joel P. Heath[4], and Zou Zou A. Kuzyk[1]

In subarctic marine environments, nutrient stocks are replenished through physical and biogeochemical processes in winter, largely setting an upper limit on new primary production for the next growing season. In spring, marine nutrient stocks are modified by freshwater-associated additions, especially in coastal areas. Hydroelectric development of the La Grande River (LGR) in northern Québec has shifted the timing of peak freshwater discharge from spring into winter, producing 10 times the natural winter discharge. Here, we considered salinity, oxygen isotope ratio ($\delta^{18}O$), and nutrient (nitrate, phosphate) data from coastal waters of northeast James Bay in different seasons of 2016 and 2017. We quantified two main freshwater sources, LGR and sea-ice melt, established by freshwater tracers, and their influence on coastal nutrient distributions. Our results show that LGR is the dominant source of freshwater to coastal waters throughout the year, especially during winter, and an important source of nitrate to nitrogen-limited coastal waters (winter concentrations of 4.53 μM versus 3.18 μM in ambient seawater). Despite being a poor phosphate source (0.11 μM versus 0.66 μM in ambient seawater), LGR provides the largest portion of the phosphate stock in surface waters near its mouth. LGR regulation has changed the pattern of natural fluvial nitrate inputs: what was observed in spring (pre-development) is now observed in winter (post-development). Thus, high winter surface nitrate stocks (22.5 mmol m^{-2}) are available to support primary production, but are dispersed to offshore areas prior to the onset of the growing season, which begins only after the return of light. In northeast James Bay, the timing and magnitude of primary production, dependent on nutrients in the water column, is expected to have been impacted by altered freshwater input, reducing overall production in local areas and potentially increasing production further downstream with cascading effects on the marine ecosystem.

Keywords: James Bay, La Grande River, Freshwater sources, Nutrients, Riverine discharge, Sea ice melt

1. Introduction

The response of marine ecosystems to environmental change in subarctic environments depends on the interactions between numerous controlling factors that include, but are not limited to, a strong seasonality in temperature, solar insolation, and consequently freshwater inputs and nutrient dynamics. These factors control many aspects of the subarctic seasonal cycle in terms of both environmental and ecological conditions. In the context of climate change, whether projected future increases in primary production in Arctic marine areas (Rysgaard et al., 1999; Arrigo et al., 2011) will be realized depends on whether freshwater additions to surface waters increase vertical stratification and decrease nutrient availability during the growing season when there is sufficient light (Tremblay and Gagnon, 2009; Bergeron and Tremblay, 2014).

In subarctic marine environments, during fall and winter, nutrients are resupplied to surface waters through vertical mixing, driven by wind and brine-induced mixing (Kuzyk et al., 2010; Granskog et al., 2011). These nutrients remain relatively unused until spring (sea-ice thinning and breakup), when increased light availability stimulates primary production in the water column and within the ice. Phytoplankton blooms typically begin in Arctic and subarctic surface waters as soon as sufficient light has returned to the under-ice environment, generally from mid-May into June (Michel et al., 1993; Mundy et al., 2011). The nutrient stock in the surface layer when spring arrives thus sets the upper limit for spring primary production, in the absence of additional nutrient sources.

[1] Centre for Earth Observation Science, University of Manitoba, Winnipeg, Manitoba, Canada

[2] Freshwater Institute, Department of Fisheries and Oceans Canada, Winnipeg, Manitoba, Canada

[3] Québec-Océan and Takuvik, Département de biologie, Université Laval, Québec, Québec, Canada

[4] The Arctic Eider Society, Sanikiluaq, Nunavut, Canada

* Corresponding author:
Email: alessia.guzzi@umanitoba.ca

Freshwater sources in coastal areas include both sea-ice (landfast) melt (SIM) and riverine discharge, a combination that influences primary production in ways that differ from the offshore ocean, where SIM is the predominant freshwater source (Prinsenberg, 1988; Carmack et al., 2015). River runoff may supply nutrients to coastal areas that are otherwise limiting in offshore waters (Granskog et al., 2005; de Melo et al., 2022; Lee et al., 2023), whereas SIM water is typically nutrient-poor (Mundy et al., 2011).

In the Canadian subarctic, Hudson Bay and its southern extension James Bay are strongly influenced by river runoff, estimated at 630–870 km^3 yr^{-1} (Saucier et al., 2004; Déry et al., 2011; Déry et al., 2016), and by SIM (annual estimate of 742 $\pm$ 10 km^3 in Landy et al., 2017; 649 km^3 in St-Laurent et al., 2011). James Bay directly receives about 300 km^3 yr^{-1} river water into an area of only 68,000 km^2 (Ridenour et al., 2019) and is relatively shallow compared to Hudson Bay (generally <40 m deep and in some places reaching 100 m deep; Martini, 1986). James Bay has been essentially unstudied in terms of freshwater and nutrient cycling since the 1970s despite extensive hydroelectric development that strongly modified the hydrology of the eastern James Bay watershed (northern Québec) and the hydrograph of major rivers including La Grande (de Melo et al., 2022).

After 50 years, oceanographic studies in James Bay have begun anew (Mundy, 2021; Peck et al., 2022; Évrard et al., 2023; Meilleur et al., 2023), in part to address community and First Nation concerns about observed environmental changes along coastal areas of the bay, including declines in seagrasses (*Zostera marina*, commonly known as eelgrass). A recent study found statistical associations between eelgrass biomass and high discharge from the regulated La Grande River (LGR), which discharges into northeast James Bay (NEJB; Leblanc et al., 2023). The objectives of this study are to alleviate persisting baseline data gaps by (1) characterizing the freshwater and nutrient (nitrate and phosphate) distributions, sources and fate in the NEJB coastal area under contemporary flow regimes during summer and winter; and (2) assessing how the modifications to LGR have affected nutrient stocks in the coastal environment. This approach provides insight into how the altered hydrography of the LGR has affected the nutrient stocks potentially available to support primary production in this area in spring. To accomplish these objectives, we quantified freshwater sources and explored the sources and fate of nutrients in the coastal waters, considering conservative mixing versus biological drawdown, and identified the limiting nutrient(s).
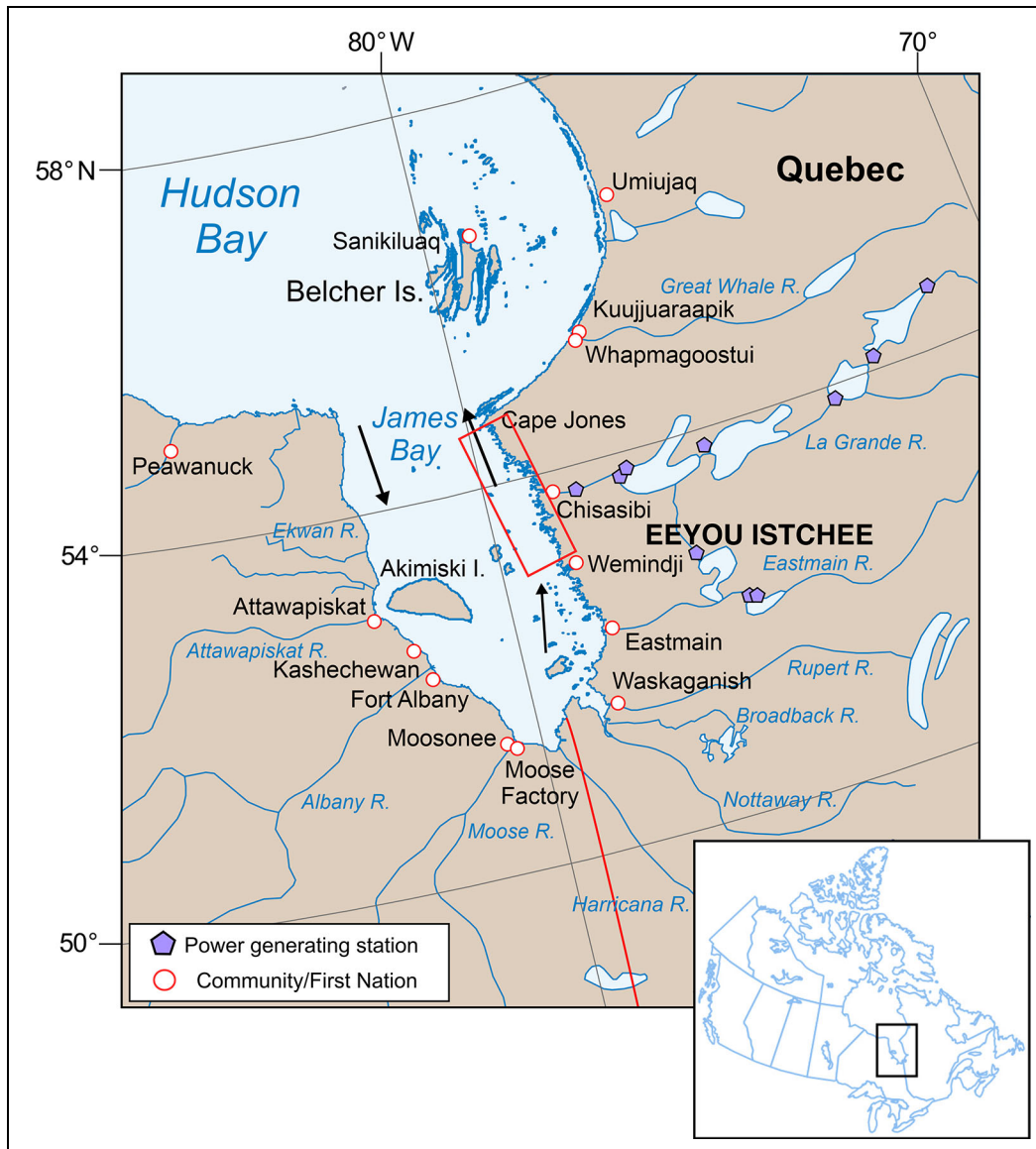
2. Study area

Hudson Bay is typically characterized as an oligotrophic system with relatively low productivity (Kuzyk et al., 2010; Ferland et al., 2011; Lapoussière et al., 2013), in large part due to the critical influence of freshwater which maintains relatively shallow, year-round stratification (Kuzyk et al., 2010; Tremblay et al., 2019). Stratification of the water column that occurs due to the addition of freshwater (SIM or riverine discharge) effectively reduces the supply of deep-water nutrients to the euphotic zone (Anderson and Roff, 1980; Roff and Legendre, 1986; Kuzyk et al., 2010; Ferland et al., 2011; Tremblay et al., 2019). Freshwater addition typically peaks between May and June in Hudson Bay (Prinsenberg, 1988), which increases the importance of riverine nutrient delivery directly to surface waters at the start of the growing season. Later in the ice-free season, when nutrients in surface waters are often depleted, and depending on the degree of wind-driven mixing, an additional nutrient source associated with continued river discharge may play an important role to support primary production (Tremblay et al., 2014).

Seawater from Hudson Bay enters James Bay along the western coast and generally circulates cyclonically within James Bay eventually exiting on the eastern coast back into Hudson Bay (**Figure 1**; Prinsenberg, 1982; Ridenour et al., 2019). As the water circulates in James Bay, it is transformed continuously by addition of freshwater, resulting in lower surface salinity on the eastern side of the Bay compared to the western side (Prinsenberg, 1984). SIM, over the area of the bay where pack ice and landfast ice are present, and riverine discharge, which generally remains constrained to the coast within the riverine coastal domain (Prinsenberg, 1988; Carmack et al., 2015), both generally impact surface salinity. A freshwater budget calculated by Prinsenberg suggests that riverine input to James Bay contributed 2.9 m of freshwater to the surface layer compared to 1.1 m of sea-ice melt from winter to summer (Prinsenberg, 1988).

James Bay is located well below the Arctic Circle, but its climate and sea-ice cycle are similar to that of continental shelves bordering the Arctic Ocean (Hochheim and Barber, 2010; 2014; Andrews et al., 2018). The climate is cold with daily average temperatures ranging from $-23.2°C$ in winter to $14.2°C$ in summer (Environment and Climate Change Canada, 2020). Sea-ice formation typically begins in November, forming across the bay area, and breakup begins in May–June, becoming ice-free typically in mid-June (Galbraith and Larouche, 2011; Taha et al., 2019; Gupta et al., 2022). Trends of both increasing and decreasing duration of landfast ice along the James Bay coast (eastern and western coasts, respectively) have been observed during the 2000–2019 period; however, the trends are strongly dependent on coastal topography and changing air temperatures (Gupta et al., 2022). On a longer time scale of 1980–2014, James Bay has been trending toward a longer open water season overall (Andrews et al., 2018).

The study area is located along the northeastern coast of James Bay between the latitudes 53.6°N and 54.6°N (**Figure 1**). The LGR was naturally the largest river along the Québec coastline; since completion of the third phase of hydroelectric development (Rupert River diversion, 2009–2012), the river now dominates regional discharge in most months of the year, and especially in winter (**Figure 2**). Prior to development the LGR annual freshwater export averaged 54 km^3 yr^{-1}, which now averages 119 km^3 yr^{-1} (de Melo et al., 2022). Flows diverted into the LGR complex originated in the Eastmain, Rupert, and Opinaca (tributary of Eastmain River) rivers of

Figure 1. Map of James Bay and surrounding areas. Inset image of James Bay's location within Canada. General circulation pattern is indicated by black arrows and the rough extent of the study area is outlined in the red rectangle. Approximate locations of power generating stations indicated with purple pentagons. White circles with red outline indicate location of First Nation communities or municipalities.

southeastern James Bay (**Figure 1**) and the Caniapiscau River, which naturally discharged into Ungava Bay (Hernández-Henríquez et al., 2010; Déry et al. 2016). Peak flows from LGR now occur between January and March (**Figure 2**), at 4000–6000 m^3 s^{-1} (Peck et al., 2022), whereas prior to development, peak discharge (approximately 3800 m^3 s^{-1} on average for 1975–1977) occurred during the spring freshet period around May–June (Messier et al., 1986; Hernández-Henríquez et al., 2010), as can be seen in all the major natural rivers around James Bay (**Figure 2**).

The sustained high flows from LGR during winter, which discharge into the landfast-ice-covered coastal environment (see **Figure 3a**), lead to the formation of a large, low surface salinity, under-ice river plume, with a "core" area (highly stratified and surface salinity < 5) of approximately 1200 km^2 and diluted waters extending throughout NEJB

to southern Hudson Bay (Eastwood et al., 2020; Peck et al., 2022). Studies in the 1980s to 2000s observed that the plume core area scaled with discharge (Ingram and Larouche, 1987; Li and Ingram, 2007), but was constrained due to the configuration of the coast and width of landfast sea ice, limiting expansion without vertical mixing. Previous studies found the depth of the core plume area to average 4–5 m (Messier et al., 1989; Peck et al., 2022). More recent increases in winter discharge have led to higher currents and a faster freshwater flushing rate through the core area. Peck et al. (2022) estimated that at mean winter discharge of 4800 m^3 s^{-1} only about 10 days are needed to fill the core plume area, such that most LGR discharge finds its way into offshore areas as well. In contrast to winter flows, the peak June flows (averaging 3094 m^3 s^{-1} over 2013–2019; P del Giorgio, personal communication, 13/02/2023), which would be the highest of the year under natural
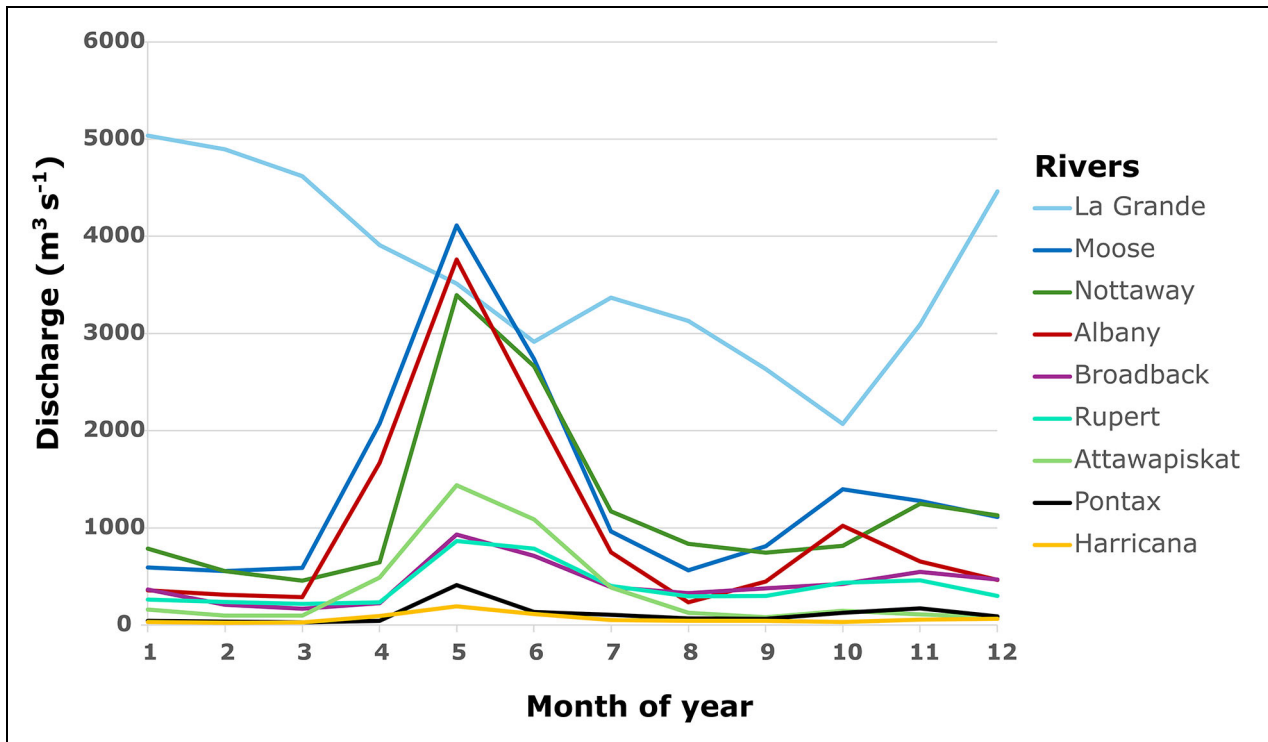
Figure 2. Average monthly discharge of nine rivers discharging into James Bay for 2017. Each river corresponds to the color in the legend. La Grande River is regulated, as well as tributaries of the Moose River (Abitibi and Mattagami rivers). Rupert and Albany rivers have been partially diverted. Historical hydrometric data (2017) was accessed through the Canadian Water Service for the Moose, Albany, Attawapiskat, and Harricana rivers. Average monthly discharge data for La Grande, Broadback, Nottaway, Pontax, and Rupert rivers were provided by the del Giorgio team (P del Giorgio, personal communication, 05/06/2024; de Melo et al., 2022).

conditions, are at the low end of the observed natural range for the spring peak (2400–6100 $m^3 s^{-1}$ for 1960–1978; Messier et al., 1986).

2.1. Background for study
This work is part of a multidisciplinary study of the eelgrass and coastal environment in NEJB entitled the Eeyou Coastal Habitat Comprehensive Research Program (Coastal Habitat Comprehensive Research Project, 2020). The NEJB region, which the LGR development has impacted, is part of the traditional territory of the Cree known as Eeyou Istchee (Cree homeland). This study was conducted in partnership with the Cree Nation of Chisasibi. Community research partners contributed to the study design and field sampling and shared knowledge about water circulation and the ice environment. A motivation for the study was the concern among Cree community members about environmental changes (MacDonald et al., 1997) and the impacts of the increased LGR plume on the health of eelgrass (*Zostera marina*), which historically occurred as vast meadows along the NEJB coast including a large embayment called Bay of Many Islands (BoMI) approximately 40 km north of the river mouth (Lalumière et al., 1994; Kuzyk et al., 2023). Eelgrass biomass and extent declined dramatically during the late 1990s and to date the meadows have failed to recover (Leblanc et al., 2023). Leblanc et al. (2023) found that high discharge from LGR, early ice breakup and warming

waters negatively affect eelgrass biomass at some beds in the NEJB area.

3. Methods
3.1. Sample collection
Water samples were collected during three periods in both 2016 and 2017, referred to as early winter (January), late winter (April), and summer (August/early September). Table S1 provides the ranges of dates when sampling was conducted. Sampling stations extended north and to a lesser extent south of the LGR where it discharges near the community of Chisasibi (**Figure 3**). All stations were within 25 km of the shore and within the limit of the landfast ice. In 2016, 38 stations were visited over three sampling trips in early winter, late winter, and summer. In 2017, 47 stations were sampled over four separate sampling trips but spanning the same three seasons. The initial location selection was informed by Marine Environmental Data Service (MEDS) surveys conducted in the early 1970s in this region, to provide a means for potential data comparison. Stations varied spatially between the 2 years because of ice conditions and a shift in focus from capturing the LGR plume extent in 2016 (north–south) to understanding its flow inshore to smaller bays known for eelgrass presence in 2017. Winter stations were decided with local guides and were often dictated by the condition and extent of landfast ice during the particular sampling trip.
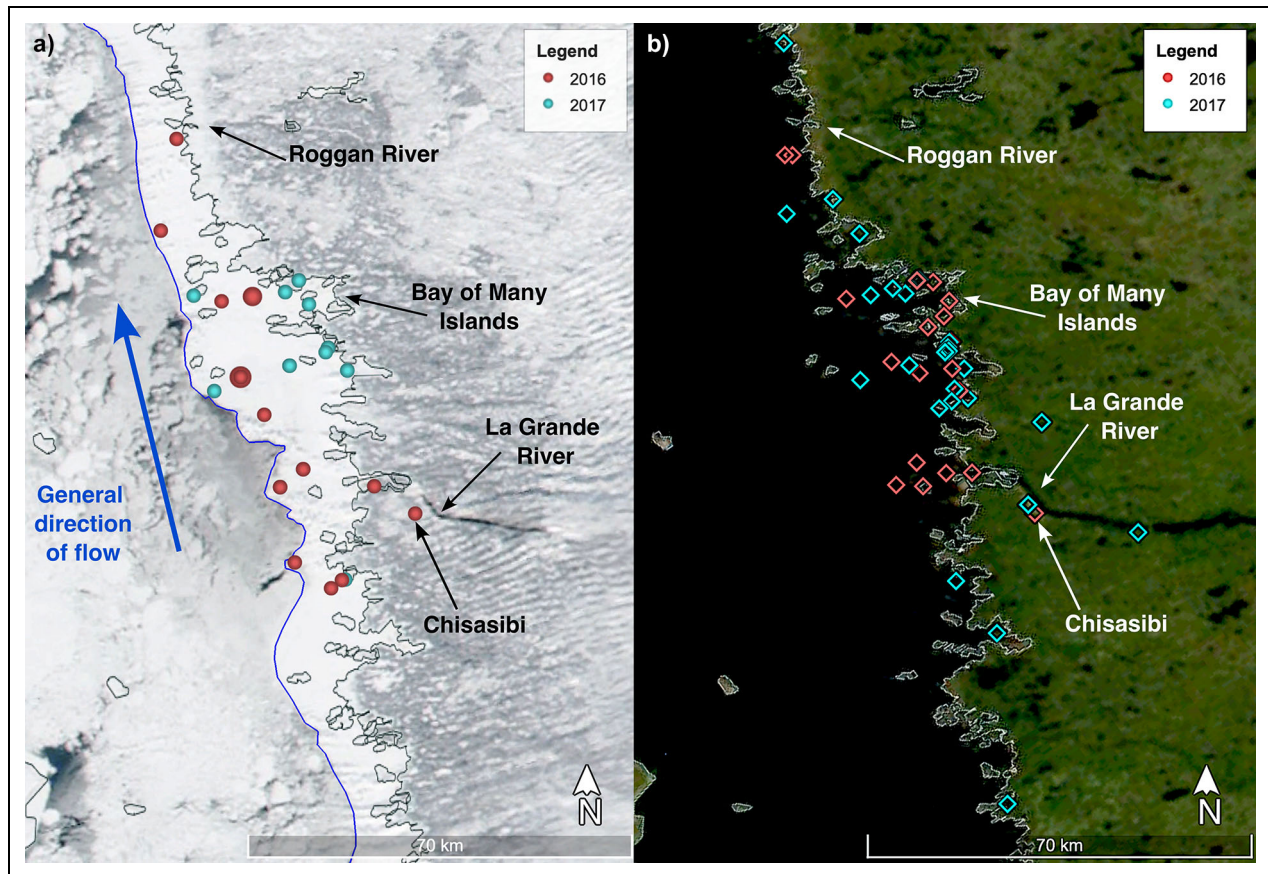
Figure 3. Maps of the sampling stations for this study in winter (a) and summer (b). Satellite images were sourced from NASA Worldview from January 20, 2016 (a) and July 4, 2017 (b). Winter stations were visited in January and April, summer stations were visited in late August and early September, and dates of sampling can be found in Table S1. Sampling stations are shown in red (2016) and blue (2017). Points that appear larger in winter indicate stations that were visited more than once. General background flow direction is identified by the blue arrow (a). In winter (a), landfast ice edge is traced in blue, mobile pack ice lies seaward of the landfast ice, and open water (flaw leads) appear as dark areas.

Winter sampling was conducted using the landfast ice as a platform. Upon arrival at a station by snowmobile, a hole was augered through the landfast ice, cleared free of slush, and then the instruments and water sampler were deployed. In summer, sampling took place from freighter canoes, with the instruments and the water sampler deployed directly from the side of the canoe. Conductivity, temperature, depth (CTD) profiles were obtained with an Idronaut Ocean Seven 304 Plus or a Sontek Castaway CTD profiler and most often with both. Instrument accuracies, as stated by the manufacturers are $\pm 0.05°C$, 0.25% ± 5 μS cm^{-1} for conductivity, and ± 0.1 for salinity for the Castaway, and $\pm 0.002°C$ and ± 0.003 mS cm^{-1} for the Idronaut Ocean Seven 304 Plus. The CTD data were used only in a supporting role in this study but are published in a parallel study on the hydrography of the plume (Peck et al., 2022).

Various depths in the water column were sampled at each site with the use of a Kemmerer water sampler, which was deployed with a pre-marked rope (1 m intervals) and a weight at the bottom to counteract the effect of currents. At stations <5 m deep, generally surface samples were collected. At all other stations, surface and near-bottom (within 1 m) water was collected. These sampling depths were determined using the Castaway CTD profiles that can be viewed immediately after casts. If a halocline was present, samples were collected within 1 m above and below the halocline (usually at near-bottom) to assess whether properties differed between layers.

3.2. Sample analysis

Water samples were processed within a few hours of collection in a temporary, clean laboratory space, free of materials that would contaminate samples. All samples were analyzed for macronutrient concentrations (nitrate and phosphate results are examined in this study), salinity, and oxygen isotope ratio ($\delta^{18}O$). Samples for $\delta^{18}O$ were collected into new 20 mL scintillation vials with no headspace, tightly capped and sealed with parafilm, and then stored at 4°C. The samples were analyzed at Ján Veizer Stable Isotope Laboratory (formerly GG Hatch) at the University of Ottawa using a Gasbench attached to a DeltaPlus XP isotope ratio mass spectrometer (ThermoFinnigan, Germany). References for analysis methods include Friedman and O'Neil (1977) and Horita et al. (1993). Subsamples (0.6 mL) were pipetted into an Exetainer and,

together with internal standards, flushed with a gas mixture of 2% CO_2 in helium using the Gasbench. Exetainers were left to equilibrate at 25°C for a minimum of 18 h. Values are expressed in standard $\delta^{18}O$ notation (in per mil or ‰ units) with the V-SMOW (Vienna Standard Mean Seawater) as reference value. Analytical instrument precision was ±0.15‰. Water samples for salinity were collected into clean 125 mL Boston Round glass bottles, tightly capped and sealed with parafilm. Salinity was measured using a Guildline Autosal 8400 salinometer with a precision better than 0.002 at the Marine Productivity Laboratory at the Freshwater Institute (FWI), Fisheries and Oceans (DFO), Winnipeg. Samples were standardized against IAPSO Standard Sea Water. Nutrient samples were collected after filtration through a pre-combusted (5 h at 500°C) glass fiber filter (25 mm Whatman GF/F, nominal pore size of 0.7 um) held in an acid-washed (10% HCl) syringe-style filter holder. The filtrate was collected into 15 mL acid-washed (10% HCl) polyethylene tubes, after three sample rinses. Samples were frozen at −20°C until samples were analyzed using a Bran and Luebbe Autoanalyzer III following standard colorimetric methods (Grasshoff et al., 1999) at Université Laval, Québec. Analytical detection limits for the nutrient concentrations used in this study are 0.03 μM for NO_3^- (nitrate) and 0.05 μM for PO_4^{3-} (phosphate).

3.3. Data analysis

To ensure accuracy of sampling depths, bottle salinity results were matched with CTD salinity readings. This matching was done to avoid discrepancies potentially caused by currents altering the depth at which the Kemmerer was ultimately closed, as the CTD and Kemmerer sampler were deployed independently. Only bottle salinity is presented in this study.

Statistical analyses were conducted with the use of R. For each property, regression analysis was used to assess whether seasonal differences were present. Analysis of covariance (ANCOVA) was used to test the significance of the variance between slopes and y-intercepts of the winter and summer salinity relationships with $\delta^{18}O$. Water mass fractions were calculated using salinity and $\delta^{18}O$ end members and a set of linear equations (see Section 3.4) and just using a salinity end member. To assess whether there was a significant difference in the fractions calculated (those calculated with salinity and $\delta^{18}O$ end members, and those just with salinity) a paired t-test was used. This test informed the final nutrient stock calculations, as described in Section 5.5.

3.4. Water mass fractions

Traditional water mass tracers, $\delta^{18}O$ and salinity, were used to distinguish between the freshening influence of river water (RW), which is fresh and isotopically light, and SIM water, which is nearly fresh and isotopically heavy, like seawater (e.g., see Tan and Strain, 1980; Östlund and Hut, 1984). We followed the method developed by Östlund and Hut (1984), wherein three linear equations are used together with a selection of end members appropriate to the dataset to calculate the fractional contributions of three source waters to each water sample (Östlund and Hut, 1984). In this study we calculated the fractions of RW, SIM, and ambient seawater (SW) for each sample.

Three linear equations to determine the fractions, F, are as follows (modified from Östlund and Hut, 1984):

$$F_{SW} + F_{RW} + F_{SIM} = 1$$

$$F_{SW}S_{SW} + F_{RW}S_{RW} + F_{SIM}S_{SIM} = S$$

$$F_{SW}X_{SW} + F_{RW}X_{RW} + F_{SIM}X_{SIM} = X$$

where F = fraction of the associated subscript, S = salinity, and X = $\delta^{18}O$. Each S and X value in the above equations represents an appropriate water type (RW, SIM, SW) end member based on this dataset. Two sets of seasonal end members were selected in this study to accurately reflect the water property conditions of winter and summer. SIM tracer data were not collected during this study period and thus we take the observed properties of sea ice in southern Hudson Bay into consideration (salinity of 0–6, and $\delta^{18}O$ between −4‰ and −0.5‰; Eastwood et al., 2020). To solve the linear equations in this study, we chose a salinity of 4.0 and a fractionation factor of 2.0‰ to calculate our representative $\delta^{18}O$, based on values and methods presented by Eastwood et al. (2020).

Sea ice provides a different signal than runoff, which can only add positive amounts of isotopically light water to the system. Sea ice freezes in winter, withdrawing freshwater from seawater that is enriched in ^{18}O and leaving salty brine behind that is depleted in ^{18}O compared to the source water. During the summer melt period, the low-salinity ice melt is returned to the water column. Accordingly, a calculated fraction of SIM in a water sample may be either positive or negative with the latter indicating a higher-than-expected salinity for the expected $\delta^{18}O$ value, which is associated with brine inputs from sea-ice formation (Granskog et al., 2011; Eastwood et al., 2020).

4. Results

4.1. Surface distributions of salinity, $\delta^{18}O$, and nutrients

During the early winters of 2016 and 2017, surface waters along the NEJB coast had very low salinities (<3) and $\delta^{18}O$ < −12‰ for 30–40 km northward of the LGR mouth. The core of the plume extended northward to the southern margin of the BoMI region. Our results show weaker stratification within the BoMI area with surface salinities of 9.6–13.6, consistent with CTD observations (Peck et al., 2022). Surface $\delta^{18}O$ reflects the observed salinity (**Figure 4a, b**) and ranged from −8.8‰ to −10.3‰. Nitrate concentrations varied from 2 μM to 5 μM, with lowest values observed in inshore waters of BoMI (**Figure 4c**). Phosphate distributions were similar to those for salinity and $\delta^{18}O$, with very low concentrations (<0.1 μM) near the river mouth and concentrations reaching 0.41 μM further north offshore of BoMI (**Figure 4d**).

Late winter surface distributions of salinity, $\delta^{18}O$, nitrate, and phosphate remained similar to early winter. Some new sampling sites south of the LGR mouth, that
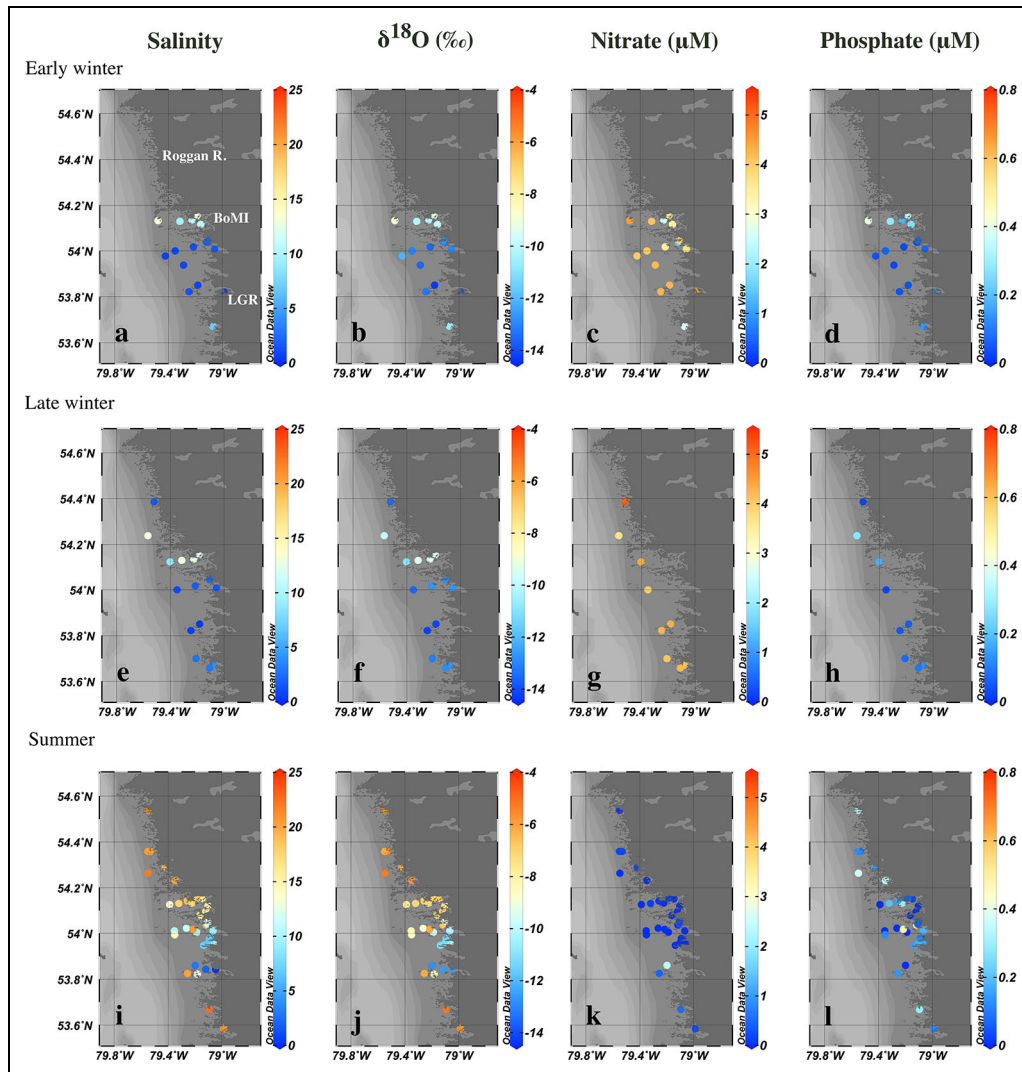
Figure 4. Maps of surface water salinity, δ¹⁸O, nitrate, and phosphate by season. Each row corresponds to a season: early winter (a–d), late winter (e–h), and summer (i–l). In (a) La Grande River (LGR), Roggan River (Roggan R.), and Bay of Many Islands (BoMI) are labeled for reference.

were visited for the first time, were found to have low surface salinity (<5) and δ¹⁸O < −12‰, nitrate between 4 μM and 5 μM, and phosphate <0.1 μM (**Figure 4e**–**h**). A new site north of BoMI near the mouth of the Roggan River showed a surface salinity of 1.8, δ¹⁸O of −13.4‰, and nitrate and phosphate concentrations of 5.1 μM and 0.4 μM, respectively.

We did not have the opportunity to revisit some of the early winter inshore sites in BoMI that had low nitrate. More stations in late winter were sampled for salinity and δ¹⁸O analysis than for nutrients (compare **Figure 4e**, **f** and **Figure 4g**, **h**).

Summer surface distributions of salinity, δ¹⁸O, nitrate, and phosphate differed from those in early and late winter. Only a few sites near the LGR had very low salinity (<5) and δ¹⁸O (<−11‰) (**Figure 4i**, **j**). Surface salinity increased rapidly with distance from the river mouth, and almost every site that was visited during both summer and winter had higher surface salinity in summer (compare **Figure 4a**, **e** and **Figure 4i**). The station near the Roggan River had a summer surface

salinity of 20.5. The median nitrate concentration in surface waters during summer was <0.01 μM (n = 45), whereas phosphate concentrations in surface waters varied from 0 to 0.45 μM with no obvious spatial pattern (**Figure 4k**, **l**).

4.2. Vertical profiles of salinity, δ¹⁸O, and nutrients

During both early winter and late winter, the water column beneath the ice cover was strongly stratified such that salinity increased abruptly with water depth. Within the core plume area, there was a fresh (salinity < 5) surface layer, about 3–5 m thick, with a sharp transition to the underlying brackish water (salinity > 15; **Figure 5a**, **e**). The observed salinity reached maximum values of 25.32 in early winter and 25.86 in late winter in the deepest waters sampled within the study area (20–25 m). The most saline subsurface samples had δ¹⁸O values during winter of −4.9‰ (**Figure 5b**, **f**). In contrast, nitrate concentrations generally decreased with depth, from surface values of about 5 μM to 2–3 μM in the deepest samples
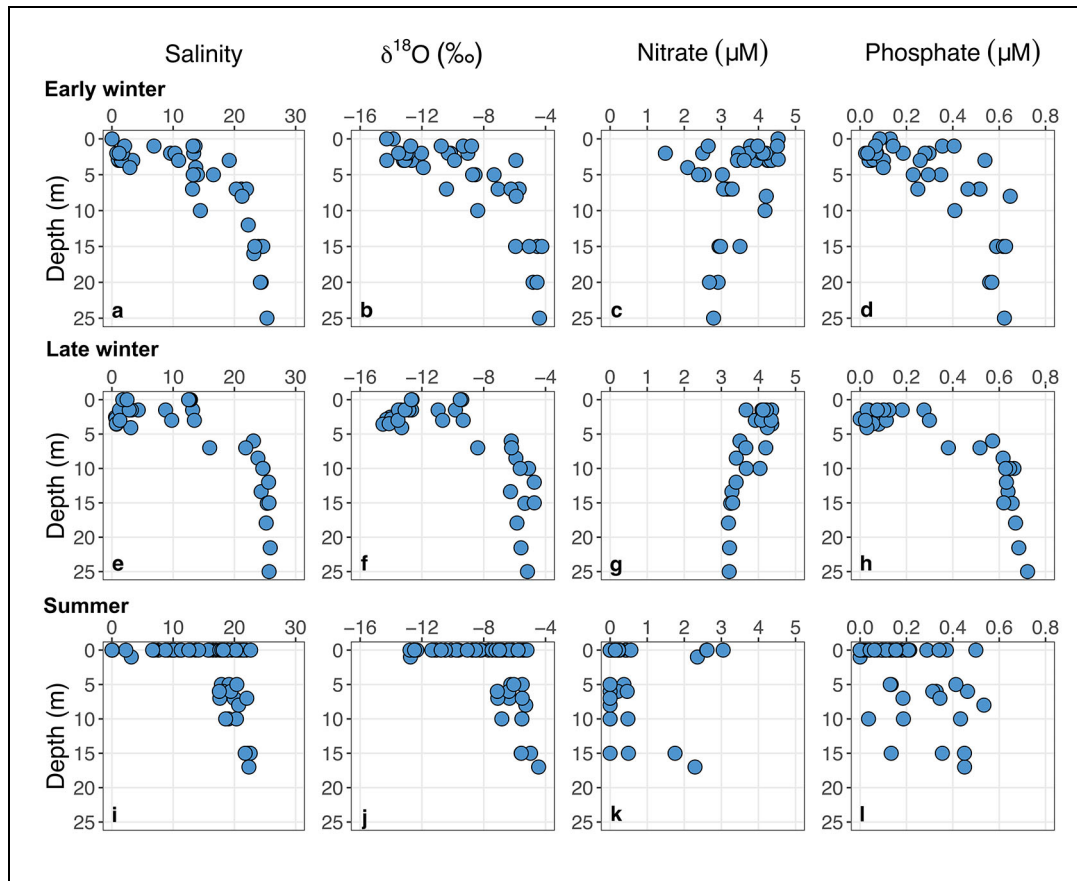
Figure 5. Salinity, δ^{18}O, nitrate, and phosphate according to depth during three seasons. Panels a–d represent early winter, panels e–h represent late winter, and panels i–l represent summer.

(**Figure 5c**, **g**). Phosphate concentrations increased with depth from surface values <0.1 µM to 0.6–0.7 µM in the deepest samples (**Figure 5d**).

During summer, we observed a wide range in salinity and δ^{18}O at the surface (top 1 m) but relatively uniform conditions in the subsurface waters (**Figure 5e**, **f**). At depths between 3 m and 10 m, salinity ranged between 17.5 and 22.0 (**Figure 5i**). Nitrate concentrations were generally lower than in both winter periods and ranged from 0 to 0.6 µM in samples from all depths except in three shallow and two deep water samples, where concentrations reached as high as 3.0 µM (**Figure 5j**). Phosphate varied between about 0 and 0.5 µM with no obvious relationship to water depth (**Figure 5i**), but subsurface values were generally lower than what was observed during winter.

4.3. δ^{18}O relationships with salinity

The linear relationship between δ^{18}O and salinity (**Figure 6**) suggests that the coastal waters of NEJB within any given season are primarily a mixture between two water types: SW that has high salinity and is enriched in ^{18}O, and RW that has zero salinity and is depleted in ^{18}O. All zero salinity samples are from the LGR, apart from one summer sample taken at an inland stream with an enriched δ^{18}O signature compared to LGR. When early
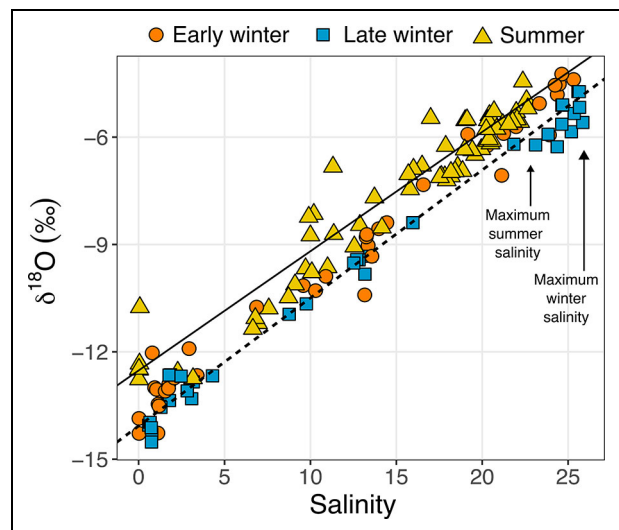
Figure 6. Relationships between δ^{18}O and salinity for the three seasons of the study. Black dashed line represents the regression for early and late winter combined (y = 0.35x − 13.83, r^2 = 0.98), and black solid line represents the regression for summer (y = 0.33x − 12.68, r^2 = 0.93). All points are colored and shaped according to the three seasons of collection. Points that fall on the salinity = 0 line are river samples.

Table 1. Average and standard deviation of salinity and $\delta^{18}O$ for La Grande River water and seawater by season

Season	Water Type	Salinity	$\delta^{18}O$ (‰)
Winter[a]	La Grande River	0.03 ± 0.01, n = 2	-14.07 ± 0.30, n = 2
	Seawater[b]	25.61 ± 0.20, n = 5	-4.92 ± 0.50, n = 5
Summer	La Grande River	0.03 ± 0.01, n = 4	-12.52 ± 0.2, n = 4
	Seawater[b]	22.45 ± 0.20, n = 4	-5.05 ± 0.50, n = 4

[a]Early and late winter data were combined to calculate average winter values.

[b]The water type seawater is representative of the most saline samples in the northeast James Bay study area.

winter and late winter samples are combined to represent the full winter season, and compared to summer samples, the $\delta^{18}O$-salinity relationship differs between seasons (**Figure 6**). The slopes of the two regressions were not significantly different (p = 0.16); however, the y-intercept of the winter regression line differed significantly from that for summer values (p < 0.001). This difference indicates a shift in the mixing line from winter to summer for both primary water types.

Table 1 provides values of the apparent end-member properties for the two primary water types considering just two seasons, winter (early and late winter combined) and summer. Freshwater samples of zero salinity collected from LGR (53.82°N, 78.99°W and 53.78°N, 78.88°W) had $\delta^{18}O$ signatures of -13.86‰ and -14.28‰ during winter, and an average of -12.52 ± 0.20‰ (n = 4) for summer. In winter, the deepest and most saline waters collected in the study area (representing SW) had an average salinity of 25.61 ± 0.20 (n = 5) and an average $\delta^{18}O$ of -4.92‰ ± 0.50 (n = 5; **Table 1**). During summer, the most saline subsurface samples had an average salinity of 22.45 ± 0.20 (n = 4) and an average $\delta^{18}O$ value of -5.05 ± 0.50‰ (n = 4; **Table 1**).

Despite a nearly three-unit difference in the salinity of SW between winter and summer, there is no significant difference in the $\delta^{18}O$ value of the most saline samples. However, the significant difference in y-intercept values (p-value < 0.001, see **Figure 6**) at -13.83‰ for winter and -12.68‰ for summer reflects the seasonal change in LGR $\delta^{18}O$ values (**Table 1**).

4.4. Nutrient relationships with salinity

In order to assess the conservativeness of nitrate and phosphate, they are compared against salinity (**Figure 7**). In **Figure 7**, salinity samples that measured zero are from the LGR at different locations and times of year, apart from one sample taken at an inland stream in summer (with 0 salinity and low nitrate and higher phosphate than other freshwater sources). Increasing salinity coincides with increasing SW contribution in the water sample.

In early and late winter there is an opposing linear pattern for nitrate and phosphate with respect to their relationships with salinity. In both winter periods, nitrate decreases and phosphate increases with increasing SW contribution (**Figure 7**). The average LGR nitrate
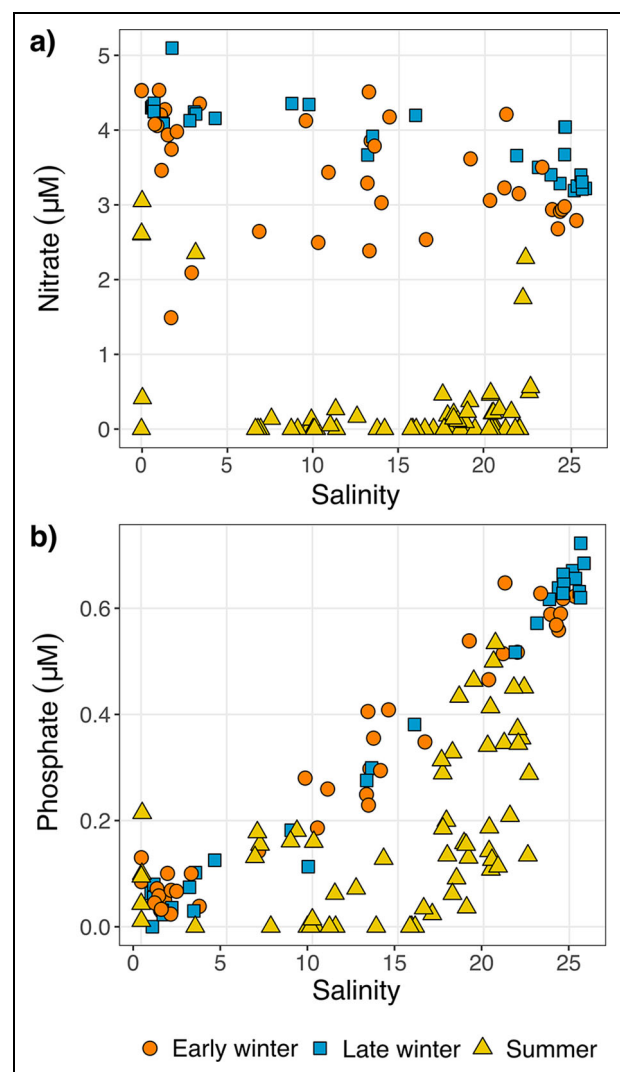
Figure 7. Seasonal relationships between (a) nitrate and salinity, and (b) phosphate and salinity. Points are colored and shaped according to season of collection (early winter, late winter, summer).

concentration in winter is higher than in SW, and the opposite is observed with phosphate (**Table 2**). Summer samples indicate a departure from the linear trends observed in winter. Table S2 provides statistical results for linear relationships by season. Nitrate and phosphate

Table 2. Average and standard deviation for La Grande River water and seawater nutrient concentrations by season

Season	Water Type	Nitrate (μM)	Phosphate (μM)
Winter[a]	La Grande River	4.53 ± 0.001, n = 2	0.11 ± 0.03, n = 2
	Seawater[b]	3.18 ± 0.2, n = 5	0.66 ± 0.04, n = 5
Summer	La Grande River	2.76 ± 0.3, n = 3	0.07 ± 0.05, n = 3
	Seawater[b]	2.29, n = 1	0.45, n = 1

[a]Early and late winter data were combined to calculate average winter values.

[b]The water type seawater is representative of the most saline samples in the northeast James Bay study area.

concentrations that represent both water types (LGR for RW, and SW) are lower in summer than what is observed in winter (**Table 2**).

5. Discussion
5.1. Seasonal differences in surface salinity along the coast
Surface salinity along the NEJB coast varied greatly between winter and summer (**Figure 4a**, **e**, **i**) largely because of differences in the thickness and extent of the plume of the LGR, which is controlled not only by the volume of river discharge but also by the reduction in wind-driven mixing in the presence of landfast ice (Messier et al., 1986; Ingram and Larouche, 1987; Messier et al., 1989; Peck et al., 2022). During 2016 and 2017, the winter discharge of the LGR averaged 4800 m^3 s^{-1} (Peck et al., 2022), which exceeded the summer discharge average of 3010 m^3 s^{-1} (de Melo et al., 2022) because of controlled discharge and increased energy demand in winter months. Previous studies have estimated a core plume extent ranging from 1200 km^2 in winter to 120 km^2 in summer (Messier et al., 1989; Peck et al., 2022), which aligns with our winter surface layer observations of salinity.

The winter water samples from BoMI lay within the region of freshwater influence of the LGR but outside the unmixed core of the plume, hence their higher surface salinities (**Figure 4a**, **e**). The study region includes many small rivers (compared to LGR) that are not expected to significantly influence the regional coastal salinity, particularly in winter when these unregulated rivers are characterized by low flow rates if they are not completely frozen (Orlova and Branfireun, 2014; de Melo et al., 2022). However, these rivers can still have a very localized impact on salinity, $\delta^{18}O$, and nutrients. For example, the low surface salinity observed near the Roggan River, located north of BoMI (**Figure 3**), was likely a result of this localized influence (**Figure 4e**, **i**). Roggan River is the second largest river in the study area, with a winter discharge of about 64 m^3 s^{-1} or 1%–2% of LGR (de Melo et al., 2022).

5.2. Temporal variation of freshwater sources
Winter isotopic depletion is typical for large northern rivers (Cooper et al., 2008; Pavlov et al., 2016) including rivers in Hudson Bay, of which several show changes of similar magnitude (about 1.5‰) between winter and summer (Granskog et al., 2011). A change in river water $\delta^{18}O$ alone would have brought about a change in both intercept *and* slope in the $\delta^{18}O$-salinity relationships, all else remaining the same. However, we found no significant difference in the slopes of the regressions between seasons (0.35‰ and 0.33‰ per unit salinity for winter and summer, respectively; **Figure 6**). The summer freshening of the SW without significant change in $\delta^{18}O$ (**Table 1**) results in the slope of the line remaining the same and the summer mixing line appearing as shifted from the winter mixing line (**Figure 6**). A limitation of the data and study design is the lack of sampling at other streams or rivers along the coast to assess the $\delta^{18}O$ signatures, except one inland stream in summer which greatly differed in $\delta^{18}O$ compared to LGR. A coastal station near Roggan River has low salinity; however, salinity was not zero in our water sample and thus we do not have a representative $\delta^{18}O$ signature for this river. Seasonal sampling conducted in 2018 and 2019 by another group shows that in winter, 15 rivers of varying sizes along the eastern coast range from −11.5‰ to −14.9‰ (P del Giorgio, personal communication, 13/02/2023). However, without enough supporting data from this study period and area, we assume that the impact of the small rivers discharging to the study area is relative to their discharge rates, and thus essentially small and negligible in comparison to LGR.

The apparent freshening of SW between winter and summer cannot be attributed to addition of RW considering the $\delta^{18}O$ values of the zero-salinity samples we obtained from the LGR. Furthermore, in the context of the regional cyclonic circulation (Prinsenberg, 1988), all sampled rivers "upstream" of the study area in southwest Hudson Bay have highly depleted $\delta^{18}O$ values similar to LGR (between −13.59‰ and −10.30‰; Granskog et al., 2011; Burt et al., 2016; Eastwood et al., 2020). Thus, we attribute the summertime freshening of the SW with no associated change in $\delta^{18}O$ to addition of SIM to the source seawater somewhere upstream of the study area.

Landfast sea ice in southern Hudson Bay is formed annually and has low salinity (typically 0–6) and $\delta^{18}O$ about 2‰ higher than that of the seawater from which it forms (Eastwood et al., 2020). To explain the summer freshening in the study area, the fractions calculated with the chosen winter end members and SIM properties imply

that the ambient winter seawater in the study area was diluted by addition of about 10%–15% SIM to produce the ambient summer seawater. This estimate of the SIM fraction in the summer water mass in NEJB exceeds a previous estimate of 5% SIM in typical Hudson Bay surface waters during summer (Granskog et al., 2011) but is in good agreement with a more recent estimate of 10% SIM for surface waters southeast of the Belcher Islands (Eastwood et al., 2020). A significant contribution of SIM to summer surface waters in northern James Bay has long been proposed (Prinsenberg, 1984) but could not be quantified with salinity as the sole tracer. The addition of SIM to surface waters may occur anywhere in Hudson Bay, but recent observations point to a potential proximal source (to James Bay) in the long-lasting sea ice that tends to accumulate due to advection from northern areas and slowly melt throughout summer in southwest Hudson Bay and northwest James Bay (Barber et al., 2021). Because of its radiative properties and feedbacks to atmospheric forcings (e.g., albedo effect), the ice typically lasts in this area well into July, and sometimes into August (see, for example, figure 2 in Etkin, 1991). Galbraith and Larouche (2011) found that this region had the latest breakup of sea ice of Hudson Bay, on average, between 1971 and 2009. Dates of ice breakup in Hudson Bay, however, have become increasingly earlier, with trends in offshore data (1980–2014) indicating earlier ice breakup by 0.51 days every year (Andrews et al., 2018).

Observations of long-lasting ice in southwestern Hudson Bay in late June 2019 revealed that it contained very thick floes (some more than 18 m) with near-zero salinity ice (Barber et al., 2021), which supports its role as a larger source of freshwater to James Bay. Protracted additions of SIM from the thick and long-lasting ice mass into the surface water flowing into northwest James Bay could explain the 10%–15% apparent SIM contribution to summer seawater observed in the NEJB study area in August, which was more than a month after the local sea ice and ice in southern James Bay had disappeared. We note that the influence of Hudson Bay SIM in NEJB may be subject to large interannual variability. As noted by Galbraith and Larouche (2011) and explored by Kirillov et al. (2022), winter ice advection has two modes: north-northwest winds coupled with reversals in the general cyclonic circulation during some winters lead to thicker ice in southern Hudson Bay, whereas enhanced west-northwest winds and cyclonic circulation in other winters lead to thicker ice in eastern Hudson Bay. An in-depth discussion about the influence of brine addition (negative SIM) in the study area between early winter and late winter can be found in the supplemental material (Text S1, Figure S1).

5.3. Influence of river water on nutrient distributions

Statistical analysis reveals that >93% of the variation in $\delta^{18}O$ observations within a particular season is explained by the mixing of RW and SW, with SIM playing a relatively smaller role. Considering its plume extent, dominance of discharge throughout the year, and the salinity-$\delta^{18}O$ relationships we observed, LGR was identified as the dominant RW source within the coastal domain of NEJB. Small and medium rivers along the eastern James Bay coast can generate local nutrient hotspots; however, LGR is known to be the largest single riverine contributor of total nitrogen and total phosphorus to James Bay, based on recent studies (de Melo et al., 2022). Thus, we proceed with using salinity alone to assess the influence of freshwater (LGR) on nutrient distributions within the study area (**Figure 7**). We avoid quantitative comparisons of those samples for which the regression residuals indicate a third freshwater source might cause large error, for example, an inland stream.

Nitrate concentrations in surface waters during late winter decreased with distance from LGR (**Figure 4g**) and decreased vertically with increasing depth in the water column (**Figure 5g**). These observations along with the significant linear relationships between nitrate and salinity ($R^2 = 0.67$, $p < 0.001$; **Figure 7a**; **Table 2**) reflect the dominant influence of the LGR on nutrient concentrations at a time of year when biological uptake was presumably negligible or very low under ice cover (Tremblay and Gagnon, 2009). During early winter, unexpectedly low nitrate concentrations at some locations within BoMI (<2.7 µM) at salinity values of 2–18 decrease the significance of the relationship ($p = 0.01$), compared to late winter. As the locations of these samples are not near enough to smaller rivers in the BoMI area to suggest dilution of the nutrient concentrations by local stream flows, we speculate that the low concentrations may be due to denitrification in sediments and/or nitrogen uptake by aquatic plants such as eelgrass (*Zostera marina*), but we have no direct evidence of either process. N* values, calculated as N* = DIN − (16 × phosphate), where DIN is dissolved inorganic nitrogen, identify the amount of nitrate needed to provide the optimal N:P ratio for phytoplankton (Gruber and Sarmiento, 1997; Tremblay et al., 2015). N represents one unit of nitrogen and P represents one unit of phosphorus, which is equivalent in one nitrate unit and one phosphate unit, respectively. Here, N and P are used interchangeably with nitrate/phosphate or nitrogen/phosphorus. N* values were calculated with our results, where DIN = nitrate concentration, and indicate that samples outside of the core plume (in BoMI and south of LGR) had a greater nitrate deficit, implying a greater likelihood of denitrification occurring compared to the core plume area (Figure S2).

Although the nitrate concentration of 4.5 µM measured in the LGR during winter was not particularly high and lies within the higher range of nine previously sampled Hudson Bay rivers in the fall season (average of 3.77 ± 2.1 µM, n = 9; Kuzyk et al., 2010), this concentration is higher than what we observe in the SW (3.18 ± 0.2 µM, n = 5; **Table 2**). The concentration in the SW was lower than what was measured in subsurface (30–50 m) residual winter waters in southern Hudson Bay (Granskog et al., 2011) and at the entrance to James Bay in fall conditions (5–7 µM; Kuzyk et al., 2010). These comparisons imply that the source waters for the NEJB coast were drawn from above 30 m water depth, which has lower nitrate concentrations (<3–4 µM) due to biological uptake

in the surface mixed layer throughout summer (Ferland et al., 2011) and poor winter nutrient replenishment because of persistent stratification by freshwater during winter (Eastwood et al., 2020).

Phosphate concentrations in coastal surface waters were <0.1 μM during winter, explained by the near-zero concentrations in LGR during winter (**Table 2**). Positive phosphate-salinity relationships during both early winter and late winter (R^2 = 0.95 and 0.98, respectively, both p < 0.001; **Figure 7**) and increasing concentrations with depth reflect higher phosphate concentrations in the SW (**Table 2**) and demonstrates the conservative relationship between the two properties.

During summer, nutrient distributions along the coast reflected both water-mass mixing and biological uptake. Despite nitrate concentrations of 2.6–3.1 μM in LGR, surface nitrate concentrations along the coast were generally very low (<0.6 μM) and often at the limit of detection (**Figure 4k**). The high surface concentrations were limited to the area closest to the river mouth. In contrast to nitrate, there was no discernible spatial pattern in surface phosphate concentrations during summer and the range of concentrations was similar to the winter periods (**Figure 4l**). These results point to nitrate (nitrogen) being the potential limiting nutrient for primary production during the summer period.

5.4. Assessment of potential macronutrient limitation

The Redfield N:P molar ratio (16:1) is used for assessing the limiting nutrient in a given system in terms of planktonic producers (Redfield, 1958). Ratios less than or greater than 16, respectively, indicate that nitrate or phosphate supply is limiting relative to the expected average nutrient demand of phytoplankton. Eelgrass (*Zostera marina*), which is abundant in the BoMI inshore waters (Lalumière et al., 1994), generally takes up nitrate and phosphate in a ratio of 20:1; overall, a mean N:P ratio of 24:1 is typically assumed for seagrass species (Duarte, 1990). There is currently no average estimate of phytoplankton nutrient demand in the study area; however, phytoplankton sampling in this region in summer and fall 1974 provide context as to what populations were present historically in the La Grande estuary (Foy and Hsiao, 1976).

During all seasons, the more saline samples were characterized by N:P ratios of about 5:1, whereas the freshest samples were characterized by ratios of about 79:1. The ratios were <237:1 across all seasons for samples with salinity < 10 (n = 42). These results suggest that in BoMI and other far-field parts of the study area, but still under the LGR influence, where surface salinities were mostly >10, nitrate would be the limiting nutrient upon the beginning of the ice-melt season (when light ceases to limit production) and in summer (data to the right of the Redfield line in **Figure 8**). This limitation could impact both phytoplankton and seagrass species, assuming no other nutrient supplements such as uptake via roots or substantial groundwater sources. Our conclusions are consistent with the pronounced drawdown of nitrate to values near the detection limit in virtually all samples
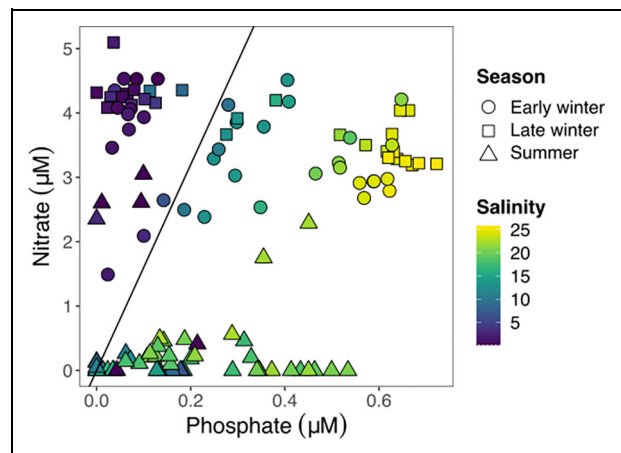
Figure 8. Seasonal relationships between nitrate and phosphate concentrations. Color gradient indicates salinity, and shapes represent season of collection: early winter (circles), late winter (squares), and summer (triangles). Solid black line represents the Redfield Ratio (N:P = 16:1).

during summer, except the very fresh samples right at the river mouth and the deepest samples (**Figure 8**). Within the core area of the winter plume (surface water salinity < 5), phosphate would be the limiting nutrient upon the beginning of the ice-melt season and throughout summer. This area of potential phosphate limitation would scale according to the plume area (1200 km^2 in winter to 120 km^2 in summer; Peck et al., 2022). These data indicate seasonality in potential nutrient limitation and spatial variability driven by plume extent.

Our finding of nitrate being the limiting macronutrient for primary production in water samples with salinity > 10 is consistent with the nitrate limitation observed widely in Arctic surface waters where the majority of N:P ratio calculations fall under 10 (datasets compiled for 2004–2016 by Ardyna et al., 2020). In coastal regions of the Mackenzie Shelf and the Beaufort Sea (summer and October–December conditions), N:P ratios in surface waters are relatively close to the Redfield ratio (13–15; Macdonald et al., 1987; Tremblay et al., 2008), whereas interior Hudson Bay is reported to have an average summer N:P ratio of 2.3 indicating extreme nitrate deficiency (Ferland et al., 2011). The SW in NEJB also demonstrates extremely oligotrophic conditions compared to southern Hudson Bay. However, the difference between NEJB and interior Hudson Bay is that the LGR discharge provides a nitrate supplement to the coastal waters.

5.5. Surface water nutrient stocks and source water contributions

Although our data suggest that LGR discharge could help alleviate nitrate limitation along the NEJB coast, evaluating the importance of LGR inputs to nutrient dynamics in the coastal domain remains difficult because of the seasonal and spatial variability of nutrient supply and demand. To assess quantitatively the nutrient contribution of LGR across space and time, two quantitative types of
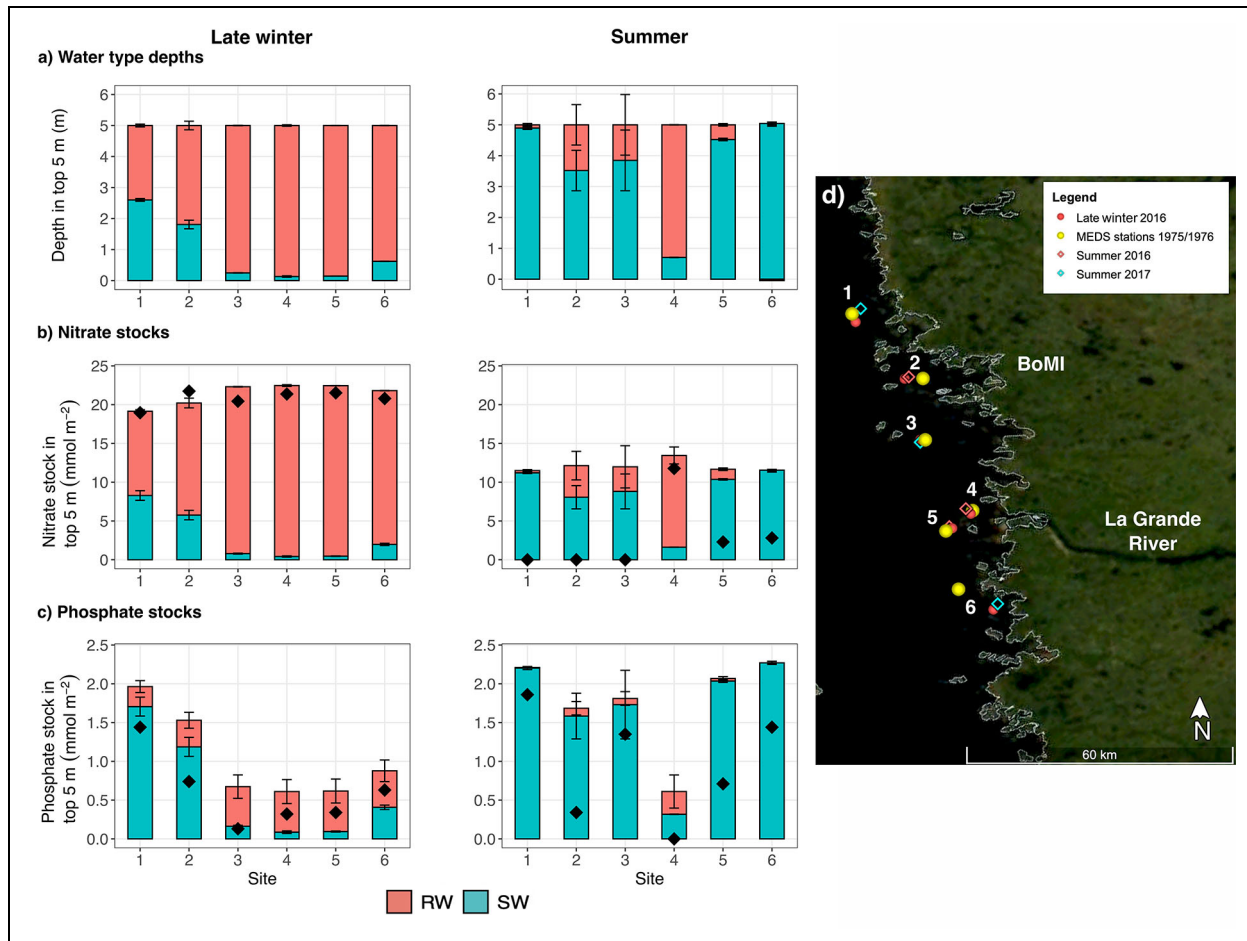
Figure 9. Water type, nitrate, and phosphate stocks in the top 5 m of the water column. Comparison of late winter and summer in terms of (a) depths of each water type, river water (RW), and seawater (SW), in the top 5 m of the water column; (b) expected stocks of nitrate in the top 5 m of the water column; and (c) expected stocks of phosphate in the top 5 m of the water column, where expected stocks represent what would be expected according to the nutrient end members (**Table 2**). Red shading shows the portion of each depth or stock derived from RW and blue shading shows the portion derived from SW. Black diamonds on each bar show the observed stocks of nutrients at each site. Error bars are representative of standard deviation, calculated through a series of error propagation equations. (d) Map of six selected sites for inventory calculations. Red points represent 2016 sites, and blue points represent 2017 sites. Yellow points represent stations from winter 1975/1976. Map sourced from NASA Worldview from July 4, 2017.

nutrient stocks were calculated for the surface layer of the water column using two quantitative methods: (i) observed stocks, based on measured nutrient concentrations integrated over a 5 m water column (the observed plume thickness in winter and the depth that showed the greatest seasonal variation in river influence); and (ii) expected stocks based on observed nutrient concentrations identified for RW and SW end members (**Table 2**), assuming no nutrient uptake. The expected nutrient stocks can be considered estimates of the initial nutrient stocks, prior to biological uptake, as a function of the combined influence of RW and SW at that location. Note that SIM was not included in stock calculations because it was a significant source of variation between winter and summer but not within each particular season. Six offshore locations (Sites 1–6; **Figure 9**) that were sampled at least once in winter and once in summer (± 3 km between seasons) were selected along the coast at

locations extending from 53 km north (Sites 1–3) to 20 km south (Site 6) of the LGR. Sites 4 and 5 are located near the LGR, with Site 5 farther removed from the river mouth and west of a small set of islands (**Figure 9**). We did not include locations that we interpreted as having been influenced by small streams during summer, based on high residuals in the salinity-$\delta^{18}O$ regression relationship.

In late winter, the surface layer of all sites was dominated by RW (**Figure 9a**). Because RW contained significant nitrate, all sites along the coast had large expected nitrate stocks of 20–24 mmol m^{-2} (**Figure 9**). The SW-derived nitrate in the surface layer increased at the sites furthest north (Sites 1 and 2) in the frontal area of the plume (Peck et al., 2022), but at most contributed 40% of the total expected nitrate stock at the northernmost site. The observed stocks of nitrate in late winter were similar to the expected stocks, consistent with the absence of significant biological drawdown.

In contrast to nitrate, phosphate stocks varied largely between sites during late winter (**Figure 9c**). Phosphate stocks were high at the northern sites with large SW supply and low at the sites nearer or south of the LGR mouth (Sites 3–6) due to low RW contribution. Observed phosphate stocks in late winter were lower than expected from conservative mixing of RW and SW. Possible explanations for this discrepancy include biological uptake of phosphate (e.g., by perennial eelgrass) or abiotic losses via processes such as sorption onto oxides in surface sediments (Sundby et al., 1992; van Raaphorst and Kloosterhuis, 1994), or sorption with iron during flocculation around the halocline in estuarine mixing zones (Macdonald et al., 1987). Dependent upon the availability of dissolved organic matter in coastal waters, bacteria may also play a role in drawdown of phosphorus. The largest difference between observed and expected phosphate concentrations were observed at Site 2, just outside of BoMI, an area known for its eelgrass beds (Lalumiere et al., 1994). However, this area is also where the LGR plume salinity increases rapidly with distance, and thus flocculation-induced phosphate losses could also be expected.

In summer, the expected nitrate stocks were about half those in late winter (**Figure 9b**), in large part due to the reduced RW contributions; they were similar across all the sites and supplied mostly by SW, except at Site 4. Phosphate stocks in summer were higher than those observed in late winter and supplied almost entirely by SW (**Figure 9c**). Again, the exception was Site 4, with a relatively low summer phosphate stock, supplied by 50% RW and 50% SW. The exceptional dominance of RW-derived nitrate at Site 4 is consistent with the phosphate limitation observed in low salinity (<10) waters (**Figure 8**) but may also be related to the relatively short residence time of LGR waters in this area in both winter (approximately 10 days; Peck et al., 2022) and summer (0.6 days). This realization of short residence time lends support to the importance of considering the stocks but also the renewal rate near the river mouth. Riverine dissolved organic nitrogen may also be a source of dissolved inorganic nitrogen through transformation processes. Additionally, areas farther away from the river mouth have different renewal rates by different processes, for example, by diffusion through the surface halocline from N-rich deeper waters.

Because summer sampling occurred late in August and thus late in the growing season, we expected to observe low summer nutrient stocks compared to expected stocks (i.e., pre-biological uptake). Except for the river mouth Site 4, observed summer nitrate stocks were drawn down to zero completely or to near-zero (**Figure 9b**). Summer phosphate stocks were also drawn down relative to expected stocks, but to varying degrees from site to site. This difference between nitrate and phosphate reinforces the notion of nitrate limitation north of LGR in summer.

5.6. Comparisons of pre- and post-development conditions

Historical data in the study area are scarce, and to our knowledge, the only available salinity and nutrient data

prior to 2016 comes from baseline studies of coastal water properties before the beginning of the La Grande Complex hydroelectric development in the late 1970s (Grainger and McSween, 1976; Messier et al., 1986; Ingram and Larouche, 1987). MEDS surveys (DFO, 2021) were conducted in the surrounding coastal and marine environment during 1974–1976. In the interest of investigating the potential effects of LGR development on freshwater and nutrient dynamics in the NEJB coastal domain (Maavara et al., 2020), we compare our results (post-development) with the data available from pre-development. Given the dearth of information available, the comparisons we can make here only capture two points in time, with no information on salinity and nutrient variability from 1978 until 2016. The following discussion highlights the observed changes and potential implications of riverine diversion and regulation.

Maximum salinity of subsurface water samples from stations near the mouth of LGR during both winter and summer (pre- and post-development) has seemingly decreased from the values reported in the 1974–1976 MEDS dataset. Our data reflect a 3-unit decrease in summer and a 2-unit decrease in winter from the 1970s. These decreases suggest that NEJB has experienced general freshening during recent decades, which aligns with indications of a climate-driven freshening trend in western Hudson Bay during the past 20–30 years based on δ^{13}C isotope trends in brachiopod shell calcite (Brand et al., 2014). However, similar analyses have not been completed for James Bay. We cannot rule out that the lower winter salinity in NEJB is locally driven, especially with the significant adjustment of the LGR hydrograph with higher flows observed in winter than during pre-development times. The lack of historical δ^{18}O data, however, means this freshening cannot be attributed to an increase in a specific freshwater source (RW and/or SIM).

The research conducted in the 1970s suggested that hydroelectric development would strongly modify seasonal flows and freshwater distributions in the coastal environment of NEJB. Based on the nutrient concentrations at the time, which suggested that the LGR did not represent a significant supply of essential nutrients (nitrate and phosphate) for primary producers in James Bay and the La Grande estuary, no changes were expected in phytoplankton production related to nutrient availability (Grainger and McSween, 1976; Messier et al., 1986). Implications of reservoir nutrient conditions and processes were not considered at the time. Reservoirs are known to act as net sinks of carbon and phosphorus; however, there is low nitrogen retention, and there may be increased mobilization of nitrogen in these altered systems (Maavara et al., 2017; Maavara et al., 2020; de Melo et al., 2022). Comparing the pre- and post-development observations, late winter nitrate concentrations associated with James Bay SW have possibly increased from the pre- to post-development periods (**Table 3**). Late winter phosphate concentrations remained similar between the two periods (**Table 3**). From this comparison we can infer that there is more RW incorporated into NEJB seawater at the regional scale during late winter, because RW is a nitrate

Table 3. Winter salinity and nutrient observations for La Grande River and east James Bay seawater

Time Period	Water Type	Salinity	Nitrate (μM)	Phosphate (μM)
Pre-development[a]	La Grande River	0[b]	1.6[c], range = 1.6–2.1, n = 16	0.15[c], range = 0.05–0.32, n = 16
	Seawater	28[b]	2.6[d]	0.68[d]
Post-development[e]	La Grande River	0.03 ± 0.01, n = 2	4.53 ± 0.001, n = 2	0.11 ± 0.03, n = 2
	Seawater	25.61 ± 0.2, n = 5	3.18 ± 0.2, n = 5	0.66 ± 0.04, n = 5

[a]Pre-development indicates the period of 1974–1978; pre-development seawater nutrient values are taken from one station at the deepest sampling depth (36.5 m).

[b]MEDS data.

[c]Messier et al. (1986).

[d]Grainger and McSween (1976).

[e]Post-development values are from this study (**Tables 1** and **2**) and included here for comparison.

source while SIM is not. Messier et al. (1986) showed average pre-development nitrate concentrations of only 1.6 μM (compared to 4.53 μM today; **Table 3**; see also de Melo et al., 2022). An exercise in calculating and comparing nutrient stocks for pre- and post-development conditions, using the method presented in Section 5.5, is included in the supplemental materials (Text S2, Figure S3) considering historical data limitations. The nutrient concentration levels imply increased N:P ratios in the LGR following development (N:P of 10.7–41.2) and increased N:P ratios in coastal waters (N:P of 3.8–4.8) that are influenced by the winter discharge. This change in nutrient ratios in any coastal system is likely to impact the community composition of primary producers, altering ecological pathways and food web transfers.

5.7. Implications of an altered NEJB coastal domain on nutrient dynamics

Nutrient distributions in the NEJB coastal domain have been modified both in space and time by the changes in LGR discharge. From this study, indicating how large-scale processes such as regional climate change and altered duration of the ice-covered season may have added to, or interacted with, the changes resulting from LGR development is not possible. However, by understanding the nitrogen cycle and land-ocean nitrogen fluxes we may gain a conceptual perspective for this study area. For example, trends of "browning" boreal rivers, carrying more terrestrial organic matter to coastal areas, may introduce greater nutrient concentrations and have implications on overall primary production (Kritzberg et al., 2020). With the majority of freshwater released into James Bay being exported from the Hudson Bay system within four years (Ridenour et al., 2019), sufficient time has elapsed for the ambient salinity to have adjusted to changes in river discharge or the sea-ice cycle that occurred over the period 1980–2012. The salinity of waters entering James Bay from Hudson Bay may have varied during these three decades as well, in view of the fluctuations in the Arctic freshwater flux (Yang et al., 2016). With scarce oceanographic data for this region, modeling could help explore the relative roles of large-scale processes and La Grande development in the apparent freshening of NEJB coastal waters (Ridenour et al., 2019; Lukovich et al., 2021). In dynamic systems such as coastal NEJB, which experiences both spatial and temporal variations of different biogeochemical properties and tracers, accurately assessing the magnitude and impact of change is difficult with the scarce data available that only represent a snapshot in time. More extensive seasonal sampling would enhance the understanding of this region, and dynamic subarctic systems similar to NEJB.

Under-ice river plumes including that of the LGR are much larger and more strongly stratified than open-water plumes for equivalent discharge because of the lack of wind mixing (Ingram and Larouche, 1987; Li and Ingram, 2007; Peck et al., 2022). Increases in winter river discharge thus act differently and more profoundly on the freshwater budgets of coastal waters than increases in discharge during ice-free periods (see also Eastwood et al., 2020). In turn, the changes in river discharge, freshwater budgets and associated mixing and stratification exert strong effects on nutrient conditions. Other recent works have emphasized the importance of the altered nutrient composition of river water following damming, showing changes to the N:P ratios in regulated river runoff and potential increases in P limitation in coastal waters (Maavara et al., 2020; de Melo et al., 2022).

Outside the core of the plume, which is 5–6 times larger than it was under the natural winter flow conditions of the 1970s (Ingram and Larouche 1987; Peck et al., 2022), there is now a larger amount of RW present in surface waters and contributing to larger nitrate stocks in late winter compared to pre-development conditions. We conclude that the development has led to a larger area of potential phosphate limitation of bacterial production in late winter and primary production once under-ice light is no longer the limiting factor. More importantly, the development has led to a buildup of nitrate stocks immediately before the productive period in what is generally a nitrate-limited system. This conclusion contrasts starkly with the pre-development conclusions by Grainger and

McSween (1976), based on limited data from natural conditions, that additional flow and more equal flow throughout the year would not have a great influence on nitrate and phosphate levels in James Bay and the La Grande estuary.

To address potential impacts on primary production, we present two potential scenarios regarding the fate of the NEJB late winter nitrate stocks, which may vary from year to year with factors such as annual riverine discharge variation and timing of ice breakup and increased sunlight. Riverine discharge can vary annually dependent upon precipitation, but also in the case of LGR, can be affected by regulation regimes and energy demand. Ice breakup typically occurs sometime in late May or early June in our study area (Taha et al., 2019), but can be as early as April, for example, as a result of storms (Peck et al., 2022). Upon breakup, the RW-derived nitrate previously confined to the surface plume is mixed into the ambient coastal waters. Trends of the landfast ice cover duration have been shown to be increasing from 2000 to 2019, with trends toward later breakup, specifically on the eastern coast of James Bay (Gupta et al., 2022); however, the offshore sea-ice season has shown a decreasing trend in James Bay from 1980 to 2014 (Andrews et al., 2018). Under a scenario of a late landfast ice breakup, there is a longer winter period for the large nitrate stocks to be exported under the landfast ice from NEJB toward and into southern Hudson Bay, possibly supporting primary production downstream. The present export of nutrients from NEJB implies that primary production in the LGR region would be lower compared to natural conditions when nitrate delivery from the rivers would have peaked with spring freshet (de Melo et al., 2022) and presumably supported larger spring phytoplankton blooms. However, varying seasonal residence times of discharge may impact the nutrient condition. For example, higher fluxes during the freshet with lower residence time may not be as important for primary production as lower fluxes in near-shore areas during summer and fall when residence times tend to be longer.

Under a scenario of early ice breakup, due to storms or to warm weather, when light conditions are suitable, we assume the large winter nitrate stocks fuel spring phytoplankton production earlier in the year. In eastern Hudson Bay, the productive period for ice algae typically occurs in April–May when sufficient light is available (Gosselin et al., 1985; Gosselin et al., 1986; Michel et al., 1988), and under-ice blooms can occur in May–June (Michel et al., 1993). In pre-development times large winter nitrate stocks would not likely have built up along the coast, as observed now, given the smaller under-ice plume with low flow conditions. The highest flows from LGR, historically, were during the spring freshet. During our study, the late winter (March–April) discharge averaged 3900–4600 $m^3 s^{-1}$, comparable to the average June discharge under natural conditions (3800 $m^3 s^{-1}$ in 1975–1977) and during freshet flows (2400–6100 $m^3 s^{-1}$ in 1960–1978; Messier et al., 1986). Thus, we propose that the current shift of peak river discharge into winter, which generates large nitrate stocks, may enhance under-ice blooms and, all

else being equal, give a competitive advantage to phytoplankton rather than rooted vascular plants like eelgrass along the NEJB coast. On the other hand, RW-associated phosphate stocks are low and thus may not support large phytoplankton blooms under the ice. To better evaluate growth conditions of eelgrass, and more generally seagrass and macroalgae, in the study area, spring nutrient stocks should be assessed together with nutrient supply from sediments.

The region of freshwater influence, surrounding the highly stratified region of the under-ice plume, has also increased in area with the increase in winter river discharge (Ingram and Larouche, 1987; Peck et al., 2022). Our results show that late winter stocks of nutrients in the region of freshwater influence originate from a combination of RW and SW, and that the late winter stock of nitrate has increased compared to pre-development conditions because of the increased RW influence. If the photosynthetic activity of ice algae is N-limited in the NEJB coastal domain, then additional RW would support increased production by the ice algal community during late winter post-development, as these algae are well adapted to low light conditions (Michel et al., 1988; Michel et al., 1996). However, increased RW content and lower salinity can also negatively impact ice algae production due to the structure of the ice itself (Granskog et al., 2005). On the other hand, the lower salinity that has been observed is within the range of toleration for eelgrass (Leblanc et al., 2023).

6. Conclusions
The data we have presented address knowledge gaps for coastal NEJB and provide a baseline with respect to SIM and RW contributions in James Bay and, by extension, the broader Hudson Bay system. In this study, we determined that the LGR is the dominant source of freshening along the NEJB coast, particularly during the winter period when SIM and other river sources are small. Summer SW is found to freshen considerably from winter, reflecting bay-wide scale increases in SIM or RW inputs. Nitrate and phosphate distributions along the NEJB coast show conservative mixing in winter but are influenced by both water mass mixing and biological nutrient uptake in summer. Evaluation of nutrient N:P ratios reveals that there is potential phosphate limitation within the core of the plume, and potential nitrate limitation outside the core of the plume, when light limitation is not a factor. The spatial boundaries of this potential nutrient limitation vary based on season and the extent of the low salinity (<10) plume. Estimates of surface nutrient stocks reveal the dominant impact of the LGR plume on nutrient conditions in winter, especially nitrate concentrations and associated stocks, which were higher than those supplied by SW. Phosphate is largely supplied in this area by SW in summer, and winter to a lesser degree. In winter months, RW from LGR is supplying the majority of the phosphate stock within the core plume area.

With the hydroelectric development of the LGR, the current winter discharge has increased 10-fold while the

natural spring freshet is held back in reservoirs and current spring/summer discharge is reduced. This shift in the hydrography has resulted in altered nutrient supply and nutrient ratios, further impacted by the landfast sea-ice cycle and associated riverine plume dynamics. We suggest future work to further assess the impact on primary production in this region, as the changes we discuss here have significant implications for the magnitude and type of primary production blooms in the NEJB coastal region, and potentially downstream in Hudson Bay.

Data accessibility statement
The raw dataset used for figures and calculations in this manuscript is publicly available on the CanWIN data repository hosted by the University of Manitoba, Centre for Earth Observation Science titled **Northeastern James Bay Water Quality Data 2016–2017**. DOI: https://doi.org/10.34992/6354-e007.

Supplemental files
The supplemental files for this article can be found as follows:

Tables S1–S2. Text S1–S2. Figures S1–S3. Docx

Acknowledgments

Funding

Competing interests
The authors have declared that no competing interests exist.

Author contributions
Contributed to conception and design: ACG, JPH, JKE, ZZAK.

Contributed to acquisition of data: ACG, JPH, JKE, ZZAK.

Contributed to analysis and interpretation of data: ACG, CM, JKE, ZZAK.

Drafted and/or revised the article: ACG, CM, JKE, JPH, JÉT, ZZAK.

Approved the submitted version for publication: All authors.

References
Anderson, JT, **Roff, JC.** 1980. Seston ecology of the surface waters of Hudson Bay. *Canadian Journal of Fisheries and Aquatic Sciences* **37**(12): 2242–2253. DOI: http://dx.doi.org/10.1139/f80-269.

Andrews, J, **Babb, D**, **Barber, DG.** 2018. Climate change and sea ice: Shipping in Hudson Bay, Hudson Strait, and Foxe Basin (1980–2016). *Elementa: Science of the Anthropocene* **6**(1): 19. DOI: http://dx.doi.org/10.1525/elementa.281.

Ardyna, M, **Mundy, CJ**, **Mills, MM**, **Oziel, L**, **Grondin, P-L**, **Lacour, L**, **Verin, G**, **van Dijken, G**, **Ras, J**, **Alou-Font, E**, **Babin, M**, **Gosselin, M**, **Tremblay, J-É**, **Raimbault, P**, **Assmy, P**, **Nicolaus, M**, **Claustre, H**, **Arrigo, KR.** 2020. Environmental drivers of under-ice phytoplankton bloom dynamics in the Arctic Ocean. *Elementa: Science of the Anthropocene* **8**(1): 30. DOI: http://dx.doi.org/10.1525/elementa.430.

Arrigo, KR, **Matrai, PA**, **van Dijken, GL.** 2011. Primary productivity in the Arctic Ocean: Impacts of complex optical properties and subsurface chlorophyll maxima on large-scale estimates. *Journal of Geophysical Research: Oceans* **116**(C11): 11022. DOI: http://dx.doi.org/10.1029/2011JC007273.

Barber, DG, **Harasyn, ML**, **Babb, DG**, **Capelle, D**, **McCullough, G**, **Dalman, LA**, **Matthes, LC**, **Ehn, JK**, **Kirillov, S**, **Kuzyk, Z**, **Basu, A**, **Fayak, M**, **Schembri, S**, **Papakyriakou, T**, **Ahmed, MMM**, **Else, B**, **Guéguen, C**, **Meilleur, C**, **Dmitrenko, I**,

Mundy, CJ, **Gupta, K**, **Rysgaard, S**, **Stroeve, J**, **Sydor, K.** 2021. Sediment-laden sea ice in southern Hudson Bay: Entrainment, transport, and biogeochemical implications. *Elementa: Science of the Anthropocene* **9**(1): 00108. DOI: http://dx.doi.org/10.1525/elementa.2020.00108.

Bergeron, M, **Tremblay, JÉ.** 2014. Shifts in biological productivity inferred from nutrient drawdown in the southern Beaufort Sea (2003–2011) and northern Baffin Bay (1997–2011), Canadian Arctic. *Geophysical Research Letters* **41**(11): 3979–3987. DOI: http://dx.doi.org/10.1002/2014GL059649.

Brand, U, **Came, RE**, **Affek, HP**, **Azmy, K**, **Mooi, R**, **Layton, K.** 2014. Climate-forced change in Hudson Bay seawater composition and temperature, Arctic Canada. *Chemical Geology* **388**: 78–86. DOI: http://dx.doi.org/10.1016/j.chemgeo.2014.08.028.

Burt, WJ, **Thomas, H**, **Miller, LA**, **Granskog, MA**, **Papakyriakou, TN**, **Pengelly, L.** 2016. Inorganic carbon cycling and biogeochemical processes in an Arctic inland sea (Hudson Bay). *Biogeosciences* **13**(16): 4659–4671. DOI: http://dx.doi.org/10.5194/bg-13-4659-2016.

Carmack, E, **Winsor, P**, **Williams, W.** 2015. The contiguous panarctic riverine coastal domain: A unifying concept. *Progress in Oceanography* **139**(19): 13–23. DOI: http://dx.doi.org/10.1016/j.pocean.2015.07.014.

Coastal Habitat Comprehensive Research Project. 2020. Canada: Niskamoon Corporation. Available at https://www.eeyoucoastalhabitat.ca/?fbclid=IwAR3QfMTyDP4Z-NBqFsO1Gea3vKIDHWtXxFaYB3UY6SeCKWkbCFGHe32aclg. Accessed November 29, 2023.

Cooper, LW, **McClelland, JW**, **Holmes, RM**, **Raymond, PA**, **Gibson, JJ**, **Guay, CK**, **Peterson, BJ.** 2008. Flow-weighted values of runoff tracers (δ^{18}O, DOC, Ba, alkalinity) from the six largest Arctic rivers. *Geophysical Research Letters* **35**(18): 3–7. DOI: http://dx.doi.org/10.1029/2008GL035007.

de Melo, ML, **Gérardin, M-L**, **Fink-Mercier, C**, **del Giorgio, PA.** 2022. Patterns in riverine carbon, nutrient and suspended solids export to the Eastern James Bay: Links to climate, hydrology and landscape. *Biogeochemistry* **161**: 291–314. DOI: http://dx.doi.org/10.1007/s10533-022-00983-z.

Déry, SJ, **Mlynowski, TJ**, **Hernández-Henríquez, MA**, **Straneo, F.** 2011. Interannual variability and interdecadal trends in Hudson Bay streamflow. *Journal of Marine Systems* **88**(3): 341–351. DOI: http://dx.doi.org/10.1016/j.jmarsys.2010.12.002.

Déry, SJ, **Stadnyk, TA**, **MacDonald, MK**, **Gauli-Sharma, B.** 2016. Recent trends and variability in river discharge across northern Canada. *Hydrology and Earth System Sciences* **20**(12): 4801–4818. DOI: http://dx.doi.org/10.5194/hess-20-4801-2016.

DFO. 2021. Marine environmental data section archive. Ecosystem and Oceans Science, Department of Fisheries and Oceans Canada. Available at https://meds-sdmm.dfo-mpo.gc.ca. Accessed October 13, 2021.

Duarte, CM. 1990. Seagrass nutrient content. *Marine Ecology Progress Series* **67**(2): 201–207. DOI: http://dx.doi.org/10.3354/meps067201.

Eastwood, RA, **Macdonald, RW**, **Ehn, JK**, **Heath, J**, **Arragutainaq, L**, **Myers, PG**, **Barber, DG**, **Kuzyk, ZA.** 2020. Role of river runoff and sea ice brine rejection in controlling stratification throughout winter in southeast Hudson Bay. *Estuaries and Coasts* **43**(4): 756–786. DOI: http://dx.doi.org/10.1007/s12237-020-00698-0.

Environment and Climate Change Canada. 2020. Canadian climate normals 1981–2010 station data: La Grande Riviere A [dataset]. Québec, Canada: ECCC. Available at https://climat.meteo.gc.ca/climate_normals/results_1981_2010_e.html?searchType=stnName&txtStationName=la+grande&searchMethod=contains&txtCentralLatMin=0&txtCentralLatSec=0&txtCentralLongMin=0&txtCentralLongSec=0&stnID=6047&dispBack=1. Accessed December 17, 2020.

Etkin, DA. 1991. Break-up in Hudson Bay: Its sensitivity to air temperatures and implications for climate warming. *Climatological Bulletin* **25**(1): 21–34.

Évrard, A, **Fink-Mercier, C**, **Galindo, V**, **Neumeier, U**, **Gosselin, M**, **Xie, H.** 2023. Regulated vs. unregulated rivers: Impacts on CDOM dynamics in the eastern James Bay. *Marine Chemistry* **256**(C7): 104309. DOI: http://dx.doi.org/10.1016/j.marchem.2023.104309.

Ferland, J, **Gosselin, M**, **Starr, M.** 2011. Environmental control of summer primary production in the Hudson Bay system: The role of stratification. *Journal of Marine Systems* **88**(3): 385–400. DOI: http://dx.doi.org/10.1016/j.jmarsys.2011.03.015.

Foy, MG, **Hsiao, SIC**. 1976. Phytoplankton data from James Bay, 1974. Report No. 631. Ste. Anne de Bellevue, Canada: Fisheries and Marine Services.

Friedman, I, **O'Neil, JR.** 1977. Compilation of stable isotope fractionation factors of geochemical interest, in Fleischer, M ed., *Data of geochemistry. 6th ed.* Washington, DC: U.S. G.P.O: KK1–KK12.

Galbraith, PS, **Larouche, P.** 2011. Sea-surface temperature in Hudson Bay and Hudson Strait in relation to air temperature and ice cover breakup, 1985–2009. *Journal of Marine Systems* **88**(3): 463–475. DOI: http://dx.doi.org/10.1016/j.jmarsys.2011.06.006.

Gosselin, M, **Legendre, L**, **Demers, S**, **Ingram, RG.** 1985. Responses of sea-ice microalgae to climatic and fortnightly tidal energy inputs (Manitounuk sound, Hudson Bay). *Canadian Journal of Fisheries and Aquatic Sciences* **42**(5): 999–1006. DOI: http://dx.doi.org/10.1139/f85-125.

Gosselin, M, **Legendre, L**, **Therriault, J-C**, **Demers, S**, **Rochet, M.** 1986. Physical control of the horizontal patchiness of sea-ice microalgae. *Marine Ecology Progress Series* **29**: 289–298. DOI: http://dx.doi.org/10.3354/meps029289.

Grainger, EH, **McSween, S.** 1976. Marine zooplankton and some physical-chemical features of James Bay related to La Grande hydro-electric development. Technical Report No. 650. Ste. Anne de Bellevue, Canada: Environment Canada, Fisheries and Marine Service.

Granskog, MA, **Kaartokallio, H**, **Thomas, DN**, **Kuosa, H.** 2005. Influence of freshwater inflow on the inorganic nutrient and dissolved organic matter within coastal sea ice and underlying waters in the Gulf of Finland (Baltic Sea). *Estuarine, Coastal and Shelf Science* **65**(1–2): 109–122. DOI: http://dx.doi.org/10.1016/j.ecss.2005.05.011.

Granskog, MA, **Kuzyk, ZZA**, **Azetsu-Scott, K**, **Macdonald, RW.** 2011. Distributions of runoff, sea-ice melt and brine using $\delta^{18}O$ and salinity data—A new view on freshwater cycling in Hudson Bay. *Journal of Marine Systems* **88**(3): 362–374. DOI: http://dx.doi.org/10.1016/j.jmarsys.2011.03.011.

Grasshoff, K, **Ehrhardt, M**, **Kremling, K**, **Anderson, LG.** 1999. *Methods of seawater analysis*. Weinheim, Germany: Wiley-VCH.

Gruber, N, **Sarmiento, JL.** 1997. Global patterns of marine nitrogen fixation and denitrification. *Global Biogeochemical Cycles* **11**(2): 235–266. DOI: http://dx.doi.org/10.1029/97GB00077.

Gupta, K, **Mukhopadhyay, A**, **Babb, DG**, **Barber, DG**, **Ehn, JK.** 2022. Landfast sea ice in Hudson Bay and James Bay. *Elementa: Science of the Anthropocene* **10**(1): 00073. DOI: http://dx.doi.org/10.1525/elementa.2021.00073.

Hernández-Henríquez, MA, **Mlynowski, TJ**, **Déry, SJ.** 2010. Reconstructing the natural streamflow of a regulated river: A case study of La Grande rivière, Québec, Canada. *Canadian Water Resources Journal* **35**(3): 301–316. DOI: http://dx.doi.org/10.4296/cwrj3503301.

Hochheim, KP, **Barber, DG.** 2010. Atmospheric forcing of sea ice in Hudson Bay during the fall period, 1980–2005. *Journal of Geophysical Research: Oceans* **115**(C5): 1–20. DOI: http://dx.doi.org/10.1029/2009JC005334.

Hochheim, KP, **Barber, DG.** 2014. An update on the ice climatology of the Hudson Bay system. *Arctic, Antarctic, and Alpine Research* **46**(1): 66–83. DOI: http://dx.doi.org/10.1657/1938-4246-46.1.66.

Horita, J, **Cole, DR**, **Wesolowski, DJ.** 1993. The activity-composition relationship of oxygen and hydrogen isotopes in aqueous salt solutions: II. Vapor-liquid water equilibration of mixed salt solutions from 50 to 100°C and geochemical implications. *Geochimica et cosmochimica acta* **57**(19): 4703–4711. DOI: http://dx.doi.org/10.1016/0016-7037(93)90194-2.

Ingram, RG, **Larouche, P.** 1987. Changes in the under-ice characteristics of La Grande rivière plume due to discharge variations. *Atmosphere-Ocean* **25**(3): 242–250. DOI: http://dx.doi.org/10.1080/07055900.1987.9649273.

Kirillov, S, **Dmitrenko, I**, **Babb, DG**, **Ehn, JK**, **Koldunov, N**, **Rysgaard, S**, **Jensen, D**, **Barber, DG.** 2022. The role of oceanic heat flux in reducing thermodynamic ice growth in Nares Strait and promoting earlier collapse of the ice bridge. *Ocean Science* **18**(5): 1535–1557. DOI: http://dx.doi.org/10.5194/os-18-1535-2022.

Kritzberg, ES, **Hasselquist, EM**, **Škerlep, M**, **Löfgren, S**, **Olsson, O**, **Stadmark, J**, **Valinia, S**, **Hansson, L-A**, **Laudon, H.** 2020. Browning of freshwaters: Consequences to ecosystem services, underlying drivers, and potential mitigation measures. *Ambio* **49**(2): 375–390. DOI: http://dx.doi.org/10.1007/s13280-019-01227-5.

Kuzyk, ZZA, **Leblanc, ML**, **O'Connor, M**, **Idrobo, J**, **Giroux, J-F**, **del Giorgio, P**, **Bélanger, S**, **Noisette, F**, **Fink-Mercier, C**, **de Melo, M**, **Walch, D**, **Ehn, J**, **Gosselin, M**, **Neumeier, U**, **Sorais, M**, **Davis, K**, **Leblon, B.** 2023. Final report from the Eeyou Coastal Habitat Comprehensive Research Project (CHCRP): Understanding Shikaapaashkw (ᓯᑳᐹᔥᐠ): Eelgrass health and goose presence in eastern James Bay. Winnipeg, Canada: Prepared for Niskamoon Corporation, University of Manitoba. DOI: http://dx.doi.org/10.34992/4K4Z-TF96.

Kuzyk, ZZA, **Macdonald, RW**, **Tremblay, J-É**, **Stern, GA.** 2010. Elemental and stable isotopic constraints on river influence and patterns of nitrogen cycling and biological productivity in Hudson Bay. *Continental Shelf Research* **30**(2): 163–176. DOI: http://dx.doi.org/10.1016/j.csr.2009.10.014.

Lalumière, R, **Messier, D**, **Fournier, J-J**, **McRoy, CP.** 1994. Eelgrass meadows in a low arctic environment, the northeast coast of James Bay, Québec. *Aquatic Botany* **47**(3–4): 303–315. DOI: http://dx.doi.org/10.1016/0304-3770(94)90060-4.

Landy, JC, **Ehn, JK**, **Babb, DG**, **Thériault, N**, **Barber, DG.** 2017. Sea ice thickness in the Eastern Canadian Arctic: Hudson Bay complex & Baffin Bay. *Remote Sensing of Environment* **200**: 281–294. DOI: http://dx.doi.org/10.1016/j.rse.2017.08.019.

Lapoussière, A, **Michel, C**, **Gosselin, M**, **Poulin, M**, **Martin, J**, **Tremblay, J-É.** 2013. Primary production and sinking export during fall in the Hudson Bay system, Canada. *Continental Shelf Research* **52**: 62–72. DOI: http://dx.doi.org/10.1016/j.csr.2012.10.013.

Leblanc, ML, **O'Connor, MI**, **Kuzyk, ZZA**, **Noisette, F**, **Davis, KE**, **Rabbitskin, E**, **Sam, LL**, **Neumeier, U**, **Costanzo, R**, **Ehn, JK**, **Babb, D**, **Idrobo, CJ**, **Gilbert, JP**, **Leblon, B**, **Humphries, MM.** 2023. Limited recovery following a massive seagrass decline in subarctic eastern Canada. *Global Change Biology* **29**(2): 432–450. DOI: http://dx.doi.org/10.1111/gcb.16499.

Lee, J, **Tefs, A**, **Galindo, V**, **Stadnyk, T**, **Gosselin, M**, **Tremblay, J-É.** 2023. Nutrient inputs from subarctic rivers into Hudson Bay. *Elementa: Science of the Anthropocene* **11**(1): 00085. DOI: http://dx.doi.org/10.1525/elementa.2021.00085.

Li, SS, **Ingram, RG.** 2007. Isopycnal deepening of an under-ice river plume in coastal waters: Field

observations and modeling. *Journal of Geophysical Research: Oceans* **112**(C7). DOI: http://dx.doi.org/10.1029/2006JC003883.

Lukovich, JV, **Jafarikhasragh, S**, **Myers, PG**, **Ridenour, NA**, **de la Guardia, LC**, **Hu, X**, **Grivault, N**, **Marson, J**, **Pennelly, C**, **Stroeve, JC**, **Sydor, K**, **Wong, K**, **Stadnyk, TA**, **Barber, DG.** 2021. Simulated impacts of relative climate change and river discharge regulation on sea ice and oceanographic conditions in the Hudson Bay Complex. *Elementa: Science of the Anthropocene* **9**(1): 00127. DOI: http://dx.doi.org/10.1525/elementa.2020.00127.

Maavara, T, **Akbarzadeh, Z**, **Van Cappellen, P.** 2020. Global dam-driven changes to riverine N:P:Si ratios delivered to the coastal ocean. *Geophysical Research Letters* **47**(15): e2020GL088288. DOI: http://dx.doi.org/10.1029/2020GL088288.

Maavara, T, **Lauerwald, R**, **Regnier, P**, **van Cappellen, P.** 2017. Global perturbation of organic carbon cycling by river damming. *Nature Communications* **8**(1): 15347. DOI: http://dx.doi.org/10.1038/ncomms15347.

MacDonald, M, **Arragutainaq, L**, **Novalinga, Z.** 1997. Voices from the Bay: Traditional ecological knowledge of Inuit and Cree in the Hudson Bay bioregion. Canadian Arctic Resource Committee. Available at https://arcticeider.com/product/voices-from-the-bay-traditional-ecological-knowledge-of-inuit-and-cree-in-the-hudson-bay-bioregion/.

Macdonald, RW, **Wong, CS**, **Erickson, PE.** 1987. The distribution of nutrients in the southeastern Beaufort Sea: Implications for water circulation and primary production. *Journal of Geophysical Research: Oceans* **92**(C3): 2939–2952. DOI: http://dx.doi.org/10.1029/JC092iC03p02939.

Martini, IP. 1986. Chapter 7 Coastal features of Canadian Inland Seas, in Martini, IP ed., *Elsevier Oceanography Series*. Elsevier: 117–142. DOI: http://dx.doi.org/10.1016/S0422-9894(08)70900-0.

Meilleur, C, **Kamula, M**, **Kuzyk, ZA**, **Guéguen, C.** 2023. Insights into surface circulation and mixing in James Bay and Hudson Bay from dissolved organic matter optical properties. *Journal of Marine Systems* **238**(4): 103841. DOI: http://dx.doi.org/10.1016/j.jmarsys.2022.103841.

Messier, D, **Ingram, RG**, **Roy, D.** 1986. Chapter 20: Physical and biological modifications in response to La Grande hydroelectric complex, in Martini, IP ed., *Canadian Inland Seas*, vol. 44. New York, NY: Elsevier: 403–424. DOI: http://dx.doi.org/10.1016/S0422-9894(08)70913-9.

Messier, D, **Lepage, S**, **de Margerie, S.** 1989. Influence du couvert de glace sur l'étendue du panache de La Grande rivière (Baie James). *Arctic* **42**(3): 278–284.

Michel, C, **Legendre, L**, **Demers, S**, **Therriault, J-C.** 1988. Photoadaptation of sea-ice microalgae in springtime: Photosynthesis and carboxylating enzymes. *Marine Ecology Progress Series* **50**: 177–185.

Michel, C, **Legendre, L**, **Ingram, RG**, **Gosselin, M**, **Levasseur, M.** 1996. Carbon budget of sea-ice algae in spring: Evidence of a significant transfer to zooplankton grazers. *Journal of Geophysical Research: Oceans* **101**(C8): 18345–18360. DOI: http://dx.doi.org/10.1029/96JC00045.

Michel, C, **Legendre, L**, **Therriault, J-C**, **Demers, S**, **Vandevelde, T.** 1993. Springtime coupling between ice algal and phytoplankton assemblages in southeastern Hudson Bay, Canadian Arctic. *Polar Biology* **13**(7): 441–449.

Mundy, CJ. 2021 Dec. ID 290: The 2021 James Bay expedition. ArcticNet Annual Scientific Meeting 2021; virtual conference. DOI: http://dx.doi.org/10.1139/as-2022-0002.

Mundy, CJ, **Gosselin, M**, **Ehn, JK**, **Belzile, C**, **Poulin, M**, **Alou, E**, **Roy, S**, **Hop, H**, **Lessard, S**, **Papakyriakou, TN**, **Barber, DG**, **Stewart, J.** 2011. Characteristics of two distinct high-light acclimated algal communities during advanced stages of sea ice melt. *Polar Biology* **34**(12): 1869–1886. DOI: http://dx.doi.org/10.1007/s00300-011-0998-x.

Orlova, J, **Branfireun, BA.** 2014. Surface water and groundwater contributions to streamflow in the James Bay Lowland, Canada. *Arctic, Antarctic, and Alpine Research* **46**(1): 236–250. DOI: http://dx.doi.org/10.1657/1938-4246-46.1.236.

Östlund, HG, **Hut, G.** 1984. Arctic Ocean water mass balance from isotope data. *Journal of Geophysical Research: Oceans* **89**(C4): 6373–6381. DOI: http://dx.doi.org/10.1029/JC089iC04p06373.

Pavlov, AK, **Stedmon, CA**, **Semushin, AV**, **Martma, T**, **Ivanov, BV**, **Kowalczuk, P**, **Granskog, MA.** 2016. Linkages between the circulation and distribution of dissolved organic matter in the White Sea, Arctic Ocean. *Continental Shelf Research* **119**: 1–13. DOI: http://dx.doi.org/10.1016/j.csr.2016.03.004.

Peck, CJ, **Kuzyk, ZZA**, **Heath, JP**, **Lameboy, J**, **Ehn, JK.** 2022. Under-ice hydrography of the La Grande River plume in relation to a ten-fold increase in wintertime discharge. *Journal of Geophysical Research: Oceans* **127**(10): e2021JC018341. DOI: http://dx.doi.org/10.1029/2021jc018341.

Prinsenberg, SJ. 1982. Present and future circulation and salinity in James Bay. *Le Naturaliste Candien* **109**: 827–841.

Prinsenberg, SJ. 1984. Freshwater contents and heat budgets of James Bay and Hudson Bay. *Continental Shelf Research* **3**(2): 191–200. DOI: http://dx.doi.org/10.1016/0278-4343(84)90007-4.

Prinsenberg, SJ. 1988. Ice-cover and ice-ridge contributions to the freshwater contents of Hudson Bay and Foxe Basin. *Arctic* **41**(1): 6–11. DOI: http://dx.doi.org/10.14430/arctic1686.

Redfield, AC. 1958. The biological control of chemical factors in the environment. *American Scientist* **46**(3): 205–221. Available at https://www-jstor-org.uml.idm.oclc.org/stable/pdf/27827150.pdf?refreqid=excelsior%3Af11611d1b19a1553954ceaab2c8b383c.

Ridenour, NA, Hu, X, Jafarikhasragh, S, Landy, JC, Lukovich, JV, Stadnyk, TA, Sydor, K, Myers, PG, Barber, DG. 2019. Sensitivity of freshwater dynamics to ocean model resolution and river discharge forcing in the Hudson Bay Complex. *Journal of Marine Systems* **196**: 48–64. DOI: http://dx.doi.org/10.1016/j.jmarsys.2019.04.002.

Roff, JC, Legendre, L. 1986. Chapter 14 Physico-chemical and biological oceanography of Hudson Bay, in Martini, IP ed., *Canadian Inland Seas*, vol. 44. New York, NY: Elsevier: 265–292. DOI: http://dx.doi.org/10.1016/S0422-9894(08)70907-3.

Rysgaard, S, Thastum, P, Dalsgaard, T, Christensen, PB, Sloth, NP. 1999. Effects of salinity on NH_4^+ adsorption capacity, nitrification, and denitrification in Danish estuarine sediments. *Estuaries* **22**(1): 21–30.

Saucier, FJ, Senneville, S, Prinsenberg, S, Roy, F, Smith, G, Gachon, P, Caya, D, Laprise, R. 2004. Modelling the sea ice–ocean seasonal cycle in Hudson Bay, Foxe Basin and Hudson Strait, Canada. *Climate Dynamics* **23**(3): 303–326.

St-Laurent, P, Straneo, F, Dumais, JF, Barber, DG. 2011. What is the fate of the river waters of Hudson Bay? *Journal of Marine Systems* **88**(3): 352–361. DOI: http://dx.doi.org/10.1016/j.jmarsys.2011.02.004.

Sundby, B, Gobeil, C, Silverberg, N, Mucci, A. 1992. The phosphorus cycle in coastal marine sediments. *Limnology and Oceanography* **37**(6): 1129–1145. DOI: https://doi.org/10.4319/lo.1992.37.6.1129.

Taha, W, Bonneau-Lefebvre, M, Bergner, AC, Tremblay, A. 2019. Evolution from past to future conditions of fast ice coverage in James Bay. *Frontiers in Earth Science* **7**: 1–20. DOI: http://dx.doi.org/10.3389/feart.2019.00254.

Tan, FC, Strain, PM. 1980. The distribution of sea ice meltwater in the eastern Canadian Arctic. *Journal of Geophysical Research: Oceans* **85**(C4): 1925–1932. DOI: http://dx.doi.org/10.1029/jc085ic04p01925.

Tremblay, J-É, Anderson, LG, Matrai, P, Coupel, P, Bélanger, S, Michel, C, Reigstad, M. 2015. Global and regional drivers of nutrient supply, primary production and CO_2 drawdown in the changing Arctic Ocean. *Progress in Oceanography* **139**: 171–196. DOI: http://dx.doi.org/10.1016/j.pocean.2015.08.009.

Tremblay, J-É, Gagnon, J. 2009. The effects of irradiance and nutrient supply on the productivity of Arctic waters: A perspective on climate change, in Nihoul, JCJ, Kostianoy, AG eds., *Influence of climate change on the changing Arctic and sub-Arctic conditions*. Dordrecht, the Netherlands: Springer: 73–94. (NATO science for peace and security series C: Environmental security). DOI: http://dx.doi.org/10.1007/978-1-4020-9460-6_1.

Tremblay, J-É, Lee, J, Gosselin, M, Bélanger, S. 2019. Nutrient dynamics and marine biological productivity in the greater Hudson Bay marine region, in Kuzyk, ZZ, Candlish, L eds., *From science to policy in the greater Hudson Bay marine region: An Integrated Regional Impact Study (IRIS) of climate change and modernization*. Québec City, Canada: ArcticNet: 225–243. Available at https://www.researchgate.net/publication/337829307.

Tremblay, J-É, Raimbault, P, Garcia, N, Lansard, B, Babin, M, Gagnon, J. 2014. Impact of river discharge, upwelling and vertical mixing on the nutrient loading and productivity of the Canadian Beaufort Shelf. *Biogeosciences* **11**(17): 4853–4868. DOI: http://dx.doi.org/10.5194/bg-11-4853-2014.

Tremblay, J-É, Simpson, K, Martin, J, Miller, L, Gratton, Y, Barber, D, Price, NM. 2008. Vertical stability and the annual dynamics of nutrients and chlorophyll fluorescence in the coastal, southeast Beaufort Sea. *Journal of Geophysical Research: Oceans* **113**(C7): 1–14. DOI: http://dx.doi.org/10.1029/2007JC004547.

van Raaphorst, W, Kloosterhuis, HT. 1994. Phosphate sorption in superficial intertidal sediments. *Marine Chemistry* **48**(1): 1–16. DOI: http://dx.doi.org/10.1016/0304-4203(94)90058-2.

Yang, Q, Dixon, TH, Myers, PG, Bonin, JA, Chambers, D, van den Broeke, MR, Ribergaard, MH, Mortensen, J. 2016. Recent increases in Arctic freshwater flux affects Labrador Sea convection and Atlantic overturning circulation. *Nature Communications* **7**(1): 10525. DOI: http://dx.doi.org/10.1038/ncomms10525.